Research Square

Preprints are preliminary reports that have not undergone peer review.
They should not be considered conclusive, used to inform clinical practice,
or referenced by the media as validated information.

Fabrication and Characterization of Hybrid Scaffolds Based on Alginate, Aloe Vera, and Polycaprolactone via 3D Printing and Electrospinning for Bone Tissue Regeneration

Sara Badr
Islamic Azad University, Science and Research Branch
Sahar amiri
polymer.amiri@gmail.com
Islamic Azad University, Science and Research Branch
Samahe Sadjadi
Iran Polymer and Petrochemical Institute
Amir Masood Rezadoust
Iran Polymer and Petrochemical Institute

Research Article

Keywords: Bone tissue engineering, Hybrid scaffold, Polycaprolactone, Sodium alginate, Electrospinning, 3D printing

Posted Date: November 24th, 2026

DOI: https://doi.org/10.21203/rs.3.rs-11705178/v1

License: This work is licensed under a Creative Commons Attribution 4.0 International License.
Read Full License

Additional Declarations: No competing interests reported.

Fabrication and Characterization of Hybrid Scaffolds Based on Alginate, Aloe Vera, and Polycaprolactone via 3D Printing and Electrospinning for Bone Tissue Regeneration

Sara Badr[1], Sahar Amiri[1]*, Samahe Sadjadi[2]*, Amir Masood Rezadoust[2]

[1] Department of Polymer Engineering, Science and Research Branch, Islamic Azad University, Tehran, Iran

[2] Gas Conversion Department, Faculty of Petrochemicals, Iran Polymer and Petrochemical Institute, Tehran, Iran

Corresponding authors:

Sahar Amiri, Email:polymer.amiri@gmail.com

Samahe Sadjadi, Email: s.sadjadi@ippi.ac.ir

Abstract

Hybrid scaffolds capable of providing mechanical support, bioactivity, and localized drug delivery are promising candidates for bone tissue engineering. In this study, multiscale hybrid scaffolds consisting of a 3D-printed polycaprolactone (PCL) framework and an electrospun poly(vinyl alcohol)/sodium alginate (PVA/SA) nanofibrous layer containing Aloe vera were fabricated and characterized. Ciprofloxacin was incorporated using two different drug-loading strategies to investigate the effect of drug localization on scaffold performance. Morphological analysis confirmed the successful formation of continuous nanofibrous structures with average fiber diameters ranging from 0.14 to 0.22 μm. Fourier-transform infrared spectroscopy verified the incorporation of Aloe vera and ciprofloxacin into the polymeric matrix, while thermogravimetric analysis demonstrated that the addition of bioactive components did not adversely affect scaffold thermal stability. In vitro cytocompatibility assessment showed that all scaffold formulations supported cell viability and exhibited a time-dependent cellular response.

Moreover, differences in ciprofloxacin localization influenced cell behavior during prolonged incubation, indicating that drug distribution within the nanofibrous layer plays an important role in scaffold–cell interactions. Overall, the developed hybrid scaffolds combined favorable physicochemical characteristics with acceptable biological performance, highlighting their potential for bone tissue regeneration and localized drug-delivery applications.

Keywords: Bone tissue engineering; Hybrid scaffold; Polycaprolactone; Sodium alginate; Electrospinning; 3D printing.

Introduction

Critical-sized bone defects remain a significant clinical challenge due to their limited capacity for spontaneous healing. Consequently, bone tissue engineering has gained considerable attention as a regenerative strategy aimed at overcoming the limitations associated with conventional bone grafting procedures [1]. Despite significant advances in biomaterial design, the development of scaffolds capable of simultaneously providing mechanical support, interconnected porosity, bioactivity, and favorable cellular interactions remains a major challenge [2]. An ideal scaffold should mimic the hierarchical structure of native bone while supporting cell attachment, nutrient transport, tissue regeneration, and gradual degradation during the healing process [3].

Various fabrication techniques have been developed to produce bone tissue engineering scaffolds, including solvent casting, gas foaming, phase separation, additive manufacturing, and electrospinning [4]. Each fabrication technique has evolved to address specific structural and functional requirements in bone tissue engineering. Each method offers specific advantages but also presents inherent limitations. Conventional porous scaffold fabrication methods often provide high porosity but limited control over pore architecture and structural reproducibility [5]. Consequently, increasing attention has been directed toward combining complementary

fabrication technologies to achieve scaffolds with both controlled macrostructure and biomimetic microstructure [6].

Among advanced scaffold fabrication technologies, additive manufacturing, particularly three-dimensional (3D) printing, has attracted considerable interest because it enables precise control of scaffold geometry, pore size, pore interconnectivity, and overall architecture [7]. Polycaprolactone (PCL) is one of the most widely used polymers for 3D-printed bone scaffolds due to its biodegradability, mechanical stability, and excellent printability [8]. However, the hydrophobic nature and limited surface bioactivity of PCL may restrict cellular interactions when it is used as a standalone material [9].

In parallel, electrospinning has emerged as an effective technique for generating nanofibrous structures that closely resemble the architecture of the extracellular matrix (ECM). Electrospun nanofibers provide a high surface-area-to-volume ratio and favorable topographical cues for cell attachment and proliferation. In addition, electrospun structures can serve as efficient carriers for bioactive molecules and therapeutic agents, enabling localized and controlled delivery within engineered tissues [10]. Natural polymers such as sodium alginate are particularly attractive for electrospun bioactive layers because of their hydrophilicity and biological compatibility [11]. Nevertheless, alginate alone exhibits poor electrospinnability and limited structural stability, which often necessitates blending with auxiliary polymers such as poly(vinyl alcohol) (PVA) to produce continuous and uniform nanofibers [12]. In addition, Aloe vera has attracted increasing interest as a natural bioactive component owing to its hydrophilic polysaccharide-rich composition and its potential to improve the biological microenvironment surrounding engineered scaffolds [13].

The integration of 3D printing and electrospinning provides a promising strategy for the fabrication of multiscale hybrid scaffolds. In such systems, a mechanically stable printed framework can provide structural support at the macroscale, while an electrospun nanofibrous coating offers a biomimetic microenvironment at the microscale and nanoscale [14]. Previous studies have demonstrated the potential of combining 3D printing and electrospinning to produce multiscale scaffolds with enhanced structural and biological properties [15]. However, most reported systems have primarily focused on architectural design and material selection, while comparatively limited attention has been devoted to understanding how the localization of therapeutic agents within different nanofibrous phases influences scaffold performance. Furthermore, studies simultaneously incorporating natural bioactive compounds and antibacterial agents within hybrid electrospun coatings remain scarce.

Building upon previous developments in hybrid scaffold design, the present study aimed to fabricate and characterize multiscale scaffolds consisting of a 3D-printed PCL framework coated with electrospun PVA/sodium alginate nanofibers containing Aloe vera and ciprofloxacin. In this study, the effect of drug localization within distinct electrospun phases was investigated while simultaneously integrating a bioactive natural component and an antibacterial agent into a hybrid scaffold platform. Two different drug-loading strategies were employed by incorporating ciprofloxacin either within the PVA phase or within the Aloe vera-containing phase. The effects of scaffold composition and drug localization on fiber morphology, surface chemistry, elemental composition, thermal behavior, and cell viability were systematically evaluated.

This study provides insight into the relationship between scaffold architecture, bioactive composition, drug incorporation strategy, and biological performance in hybrid systems intended for bone tissue engineering applications.

Materials and Methods

Materials

Polycaprolactone filament (PCL, 1.75 mm diameter, eSUN, China), poly(vinyl alcohol) (PVA, Mw ≈ 72,000 g/mol, Merck, Germany), sodium alginate (SA, food grade, purity ≥99%, PGT, China), citric acid monohydrate (ACS grade, Merck, Germany), ciprofloxacin hydrochloride injectable solution (20 mg/mL, Sina Darou, Iran), Aloe vera extract powder (200:1 extract ratio, purity ≥99%, Salvaito Aloe), phosphate-buffered saline (PBS, Medicago), acetic acid (glacial, Merck, Germany), sodium acetate (analytical grade, Merck, Germany), sodium hydroxide (analytical grade, Merck, Germany), and deionized water were used as received without further purification.

Preparation of Polymer Solutions

A 10 wt% PVA solution was prepared by dissolving PVA in deionized water under magnetic stirring (800 rpm) with mild heating, followed by overnight stirring at room temperature to ensure complete hydration. A 1 wt% SA solution was prepared in deionized water under similar stirring conditions without heating and was allowed to hydrate for 24 h to ensure homogeneity.

Aloe vera stock solutions (10 and 20 wt%) were prepared in deionized water using high-shear stirring, followed by gentle mixing at room temperature for 1.5 h. Citric acid (3 wt% of the total polymer content) was introduced as a crosslinking agent during the final stage of solution preparation under stirring for 30 min to ensure homogeneous distribution [16]. PBS solution and a 1 M NaOH aqueous solution were prepared in deionized water and used for scaffold washing and surface modification procedures.

Formulation of Polymeric Systems

To evaluate compositional effects on electrospinnability and scaffold performance, three types of systems were designed.

Binary systems (PVA/SA). SA:PVA ratios of 50:50, 60:40, 70:30, and 80:20 were prepared to evaluate fiber formation and solution stability.

Ternary systems (PVA/SA/Aloe vera). Aloe vera stock solutions were incorporated into selected binary systems. Following preliminary optimization studies, an Aloe vera content corresponding to 7 wt% of the total formulation was selected for subsequent experiments, as higher loadings adversely affected jet stability during electrospinning.

Functional systems. Based on the optimization studies, four final formulations were selected for scaffold fabrication and characterization: (a) PVA/SA/CA, (b) PVA/SA/CA/AV, (c) PVA/SA/CA/AV+CIP, in which ciprofloxacin was incorporated into the Aloe vera phase, and (d) PVA+CIP/SA/CA/AV, in which ciprofloxacin was incorporated into the PVA phase. All other formulation and processing parameters were kept constant to evaluate the effects of scaffold composition and drug localization.

Fabrication of 3D-Printed PCL Scaffolds

Scaffold frameworks were fabricated using fused deposition modeling (FDM). Prior to printing, PCL filaments were dried at 40–50 °C for 60 min to remove residual moisture and stored under desiccated conditions until use. Printing parameters included a nozzle temperature of 85 °C, a bed temperature of 35 °C, a nozzle diameter of 0.5 mm, and an extrusion width of 0.5 mm. The scaffolds were designed as cylindrical structures with a diameter of 30 mm and a height of 4 mm. The scaffold architecture was designed to generate an interconnected macroporous network capable of facilitating nutrient transport and subsequent nanofiber deposition throughout the

printed structure. A layer height of 0.2 mm was used throughout the printing process. A rectilinear infill pattern with 50% infill density and alternating 0°/90° deposition angles was applied to produce a regular interconnected pore network and improve structural uniformity throughout the scaffold. Toolpath generation was performed using Simplify3D software, while extrusion multiplier and retraction settings were maintained at their default stable values and kept constant throughout all printing experiments. The printed scaffolds subsequently served as the macroporous framework for electrospun nanofiber deposition.

Surface Modification of 3D-Printed Scaffolds

To improve nanofiber adhesion, 3D-printed PCL scaffolds were washed twice with PBS (15 min each), followed by treatment in a 1 M NaOH aqueous solution for 1 h to enhance surface roughness and surface energy [17]. After neutralization with PBS rinsing, scaffolds were air-dried prior to electrospinning.

Electrospinning Process

Nanofibrous layers were produced using a Full Option Lab ES II-I electrospinning system (NanoAzma, Iran). Electrospinning was performed using an applied voltage of 22 kV, a flow rate of 0.85 mL/h, and a tip-to-collector distance of 15 cm. Fibers were collected on a rotating drum collector (150 rpm) for 1 h and subsequently deposited onto 3D-printed scaffolds, forming a continuous and uniform nanofibrous coating.

Fabrication of Hybrid Scaffolds

The final hybrid scaffold was obtained by integrating the 3D-printed PCL framework with electrospun PVA/SA/Aloe vera nanofibers. This multiscale architecture provided mechanical support from the macroporous structure together with bioactive functionality from the nanofibrous surface.

Characterization

The fabricated scaffolds were characterized using complementary physicochemical and biological techniques to evaluate their morphology, elemental composition, chemical structure, thermal behavior, and cytocompatibility.

Fourier-transform infrared (FTIR) spectroscopy (Nexus 870, Thermo Nicolet, USA) was used to investigate functional groups, intermolecular interactions, and possible evidence of crosslinking and ciprofloxacin incorporation within the polymeric matrix [18].

The morphology, microstructure, and elemental composition of the 3D-printed, electrospun, and hybrid scaffolds were examined using scanning electron microscopy (SEM, VEGA, TESCAN, Czech Republic) equipped with an energy-dispersive X-ray spectroscopy (EDX, INCA, Oxford Instruments, UK) system. SEM provided detailed information on surface architecture and fiber distribution, while EDX analysis was used to evaluate elemental composition and identify characteristic elements associated with scaffold components, particularly the presence of nitrogen associated with ciprofloxacin incorporation [19].

Thermal behavior and degradation profiles were analyzed using thermogravimetric analysis (TGA, TG 209 F1 Iris, NETZSCH, Germany). The measurements were performed from 25 to 900 °C at a heating rate of 10 °C/min under a nitrogen atmosphere. Approximately 10 mg of each scaffold sample was placed in an alumina crucible, and mass changes were recorded as a function of temperature. The obtained thermogravimetric (TG) and derivative thermogravimetric (DTG) curves were used to evaluate the thermal stability and degradation behavior of the fabricated hybrid scaffolds.

Cellular response was assessed using the MTT assay to evaluate the viability and metabolic activity of human osteoblast-like MG-63 cells cultured in direct contact with the scaffolds [20].

Briefly, 50,000 cells were seeded in each well containing scaffold samples and incubated at 37 °C under a humidified atmosphere with 5% CO_2. After 12, 48, and 72 h of incubation, cell viability was determined using an MTT solution (0.5 mg/mL), and absorbance was measured at 570 nm. The obtained results were used to compare cytocompatibility and evaluate the time-dependent effect of scaffold composition and ciprofloxacin loading on cell behavior.

Results and Discussion

The stepwise fabrication process of the multiscale hybrid scaffold, including 3D printing of the PCL macroporous framework, surface modification, and subsequent electrospinning of the bioactive nanofibrous layer, is illustrated in Figure 1. Initially, electrospinning parameters were optimized using aluminum foil collectors to achieve continuous and uniform nanofibers before deposition onto the PCL framework. The optimized conditions were subsequently applied for nanofiber deposition onto the 3D-printed PCL scaffolds, resulting in the formation of the final hybrid architecture.

Multiple scaffold specimens from each formulation were independently fabricated under identical processing conditions to evaluate the consistency and reproducibility of the combined 3D printing and electrospinning approach. The obtained scaffolds exhibited comparable structural integrity and morphological features among independently fabricated specimens, demonstrating the consistency of the fabrication procedure.

SEM and EDX analyse were employed to investigate surface morphology, fiber distribution, and elemental composition. FTIR analysis was used to evaluate the chemical structure and possible interactions among scaffold components. TGA/DTG analysis was conducted to assess thermal stability and thermal decomposition behavior, while MTT assays were performed to evaluate the cytocompatibility and time-dependent cellular response of the fabricated scaffolds.

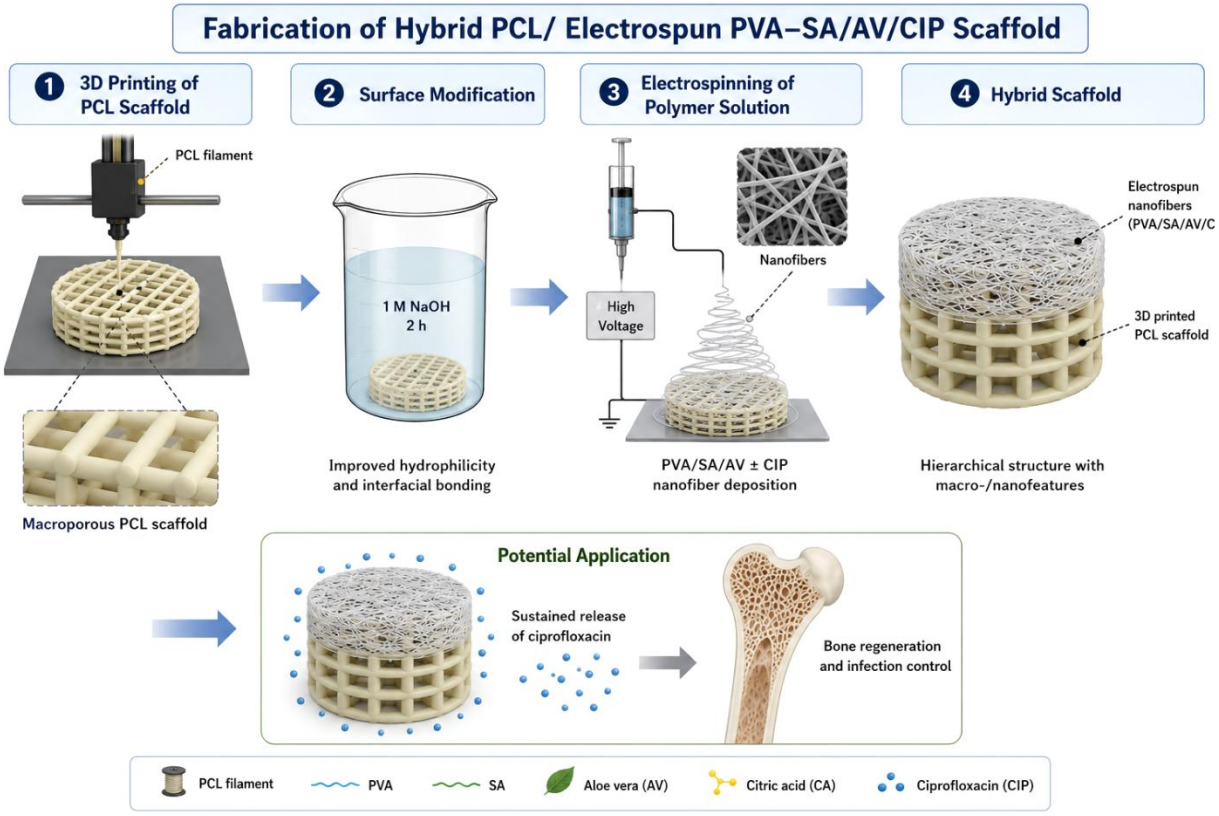

Figure 1. Schematic illustration of the fabrication process of the multiscale hybrid scaffold, including 3D printing of the PCL macroporous framework, surface modification, electrospinning of PVA/sodium alginate/Aloe vera nanofibrous layers with ciprofloxacin incorporation, and formation of the final hybrid scaffold with hierarchical macro/nanostructure.

Optimization of the Electrospinning Process

To determine the optimal polymer composition for electrospinning, a series of formulations including pure PVA, pure SA, and binary PVA/SA blends were systematically investigated. To evaluate the intrinsic electrospinnability of the polymer solutions independently of scaffold geometry, all fibers were initially collected on aluminum foil. The resulting morphologies were analyzed using SEM (Figure 2).

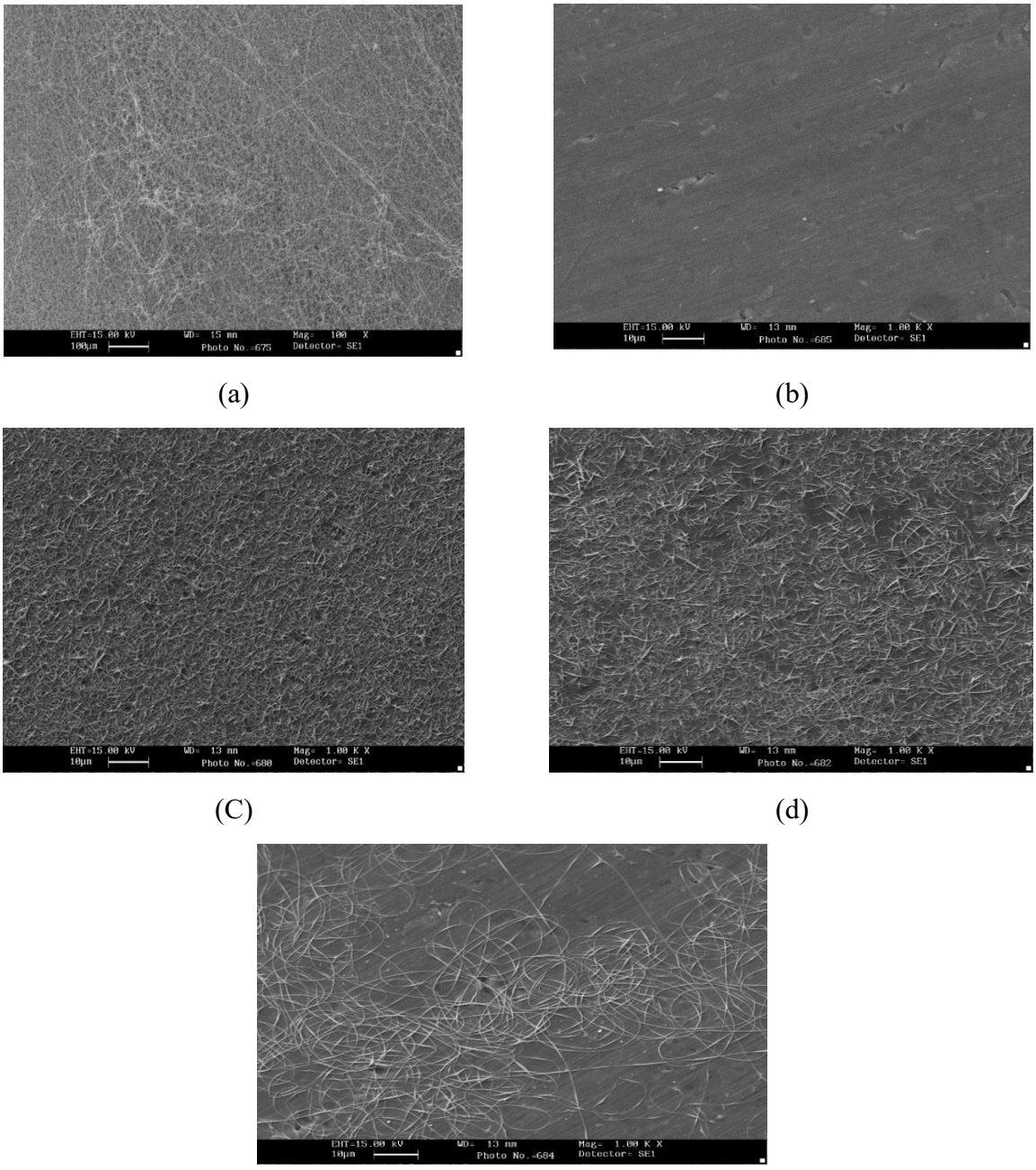

Figure 2. SEM images of electrospun fibers collected on aluminum foil: (a) pure PVA, (b) pure SA, (c) SA/PVA (70:30), (d) SA/PVA (60:40), and (e) SA/PVA (50:50), demonstrating the effect of polymer ratio on fiber morphology and electrospinnability.

Pure PVA exhibited continuous, bead-free nanofibers with uniform morphology, confirming its favorable spinnability and suitability as a carrier polymer for fiber formation [21]. In contrast,

pure SA failed to form continuous fibers and instead produced fragmented and bead-dominated structures. This behavior is attributed to its high charge density and insufficient chain entanglement, which limit stable jet formation during electrospinning [22].

To improve fiber formation while retaining the bioactivity of alginate, binary SA/PVA systems were prepared at different weight ratios (70:30, 60:40, and 50:50). SEM analysis revealed a composition-dependent trend in fiber morphology. Increasing SA content resulted in progressive deterioration of fiber uniformity, manifested by increased bead formation, fiber breakage, and diameter heterogeneity.

Among the tested formulations, the 50:50 PVA/SA blend demonstrated the most suitable fiber morphology, showing relatively uniform nanofiber formation while maintaining sufficient alginate content for biofunctional relevance. In contrast, formulations containing higher SA content (70:30 and 60:40 SA/PVA ratios) exhibited increased morphological irregularities, whereas excessive alginate incorporation led to significant disruption of fiber continuity.

Based on these observations, the 50:50 PVA/SA ratio was selected as the optimal base formulation for subsequent incorporation of Aloe vera and ciprofloxacin. These findings highlight the role of PVA in promoting electrospinning stability through enhanced chain entanglement and viscoelastic support, whereas increasing alginate content reduced solution spinnability and fiber uniformity [23].

Morphological and Elemental Characterization of Hybrid Scaffolds

Morphological and Elemental Analysis of the Base Hybrid Scaffold (PCL + SA/PVA/CA)

The morphology and microstructure of the base hybrid scaffold were investigated by SEM to evaluate the architecture of the 3D-printed substrate, the continuity of the electrospun nanofibrous layer, and the structural integration between the two phases. To minimize

processing-related variability, all PCL substrates were fabricated under identical printing conditions, providing a consistent macroporous framework for subsequent electrospinning. In parallel, EDX was employed to examine the elemental composition of both the overall scaffold and the electrospun layer.

The crosslinked SA/PVA system containing citric acid was used as the base nanofibrous formulation. SEM micrographs demonstrated that the 3D-printed PCL substrate possessed a regular interconnected porous architecture with well-defined filament organization and open pore geometry (Fig. 3a,d). The pore size ranged from 0.58 to 0.80 mm, with an average value of approximately 0.67 mm, confirming the formation of a controlled macroporous structure with potential suitability for nutrient transport and cell infiltration [24]. Following electrospinning, a continuous nanofibrous network was deposited across both the filament surfaces and pore regions of the scaffold (Fig. 3b,c). The electrospun layer formed a homogeneous coating while maintaining pore interconnectivity, indicating stable fiber deposition without significant pore blockage. At higher magnifications, localized regions of increased fiber density were observed, likely resulting from overlapping fiber accumulation during electrospinning. Representative fiber diameter measurements revealed values ranging from 0.18 to 0.29 μm, with an average diameter of 0.22 ± 0.06 μm (Fig. 3e).

EDX analysis further confirmed the expected elemental composition of the hybrid scaffold. The cumulative spectrum obtained from the overall scaffold surface exhibited dominant carbon and oxygen peaks, corresponding to the polymeric composition of both the PCL substrate and the electrospun layer (Fig. 3f).

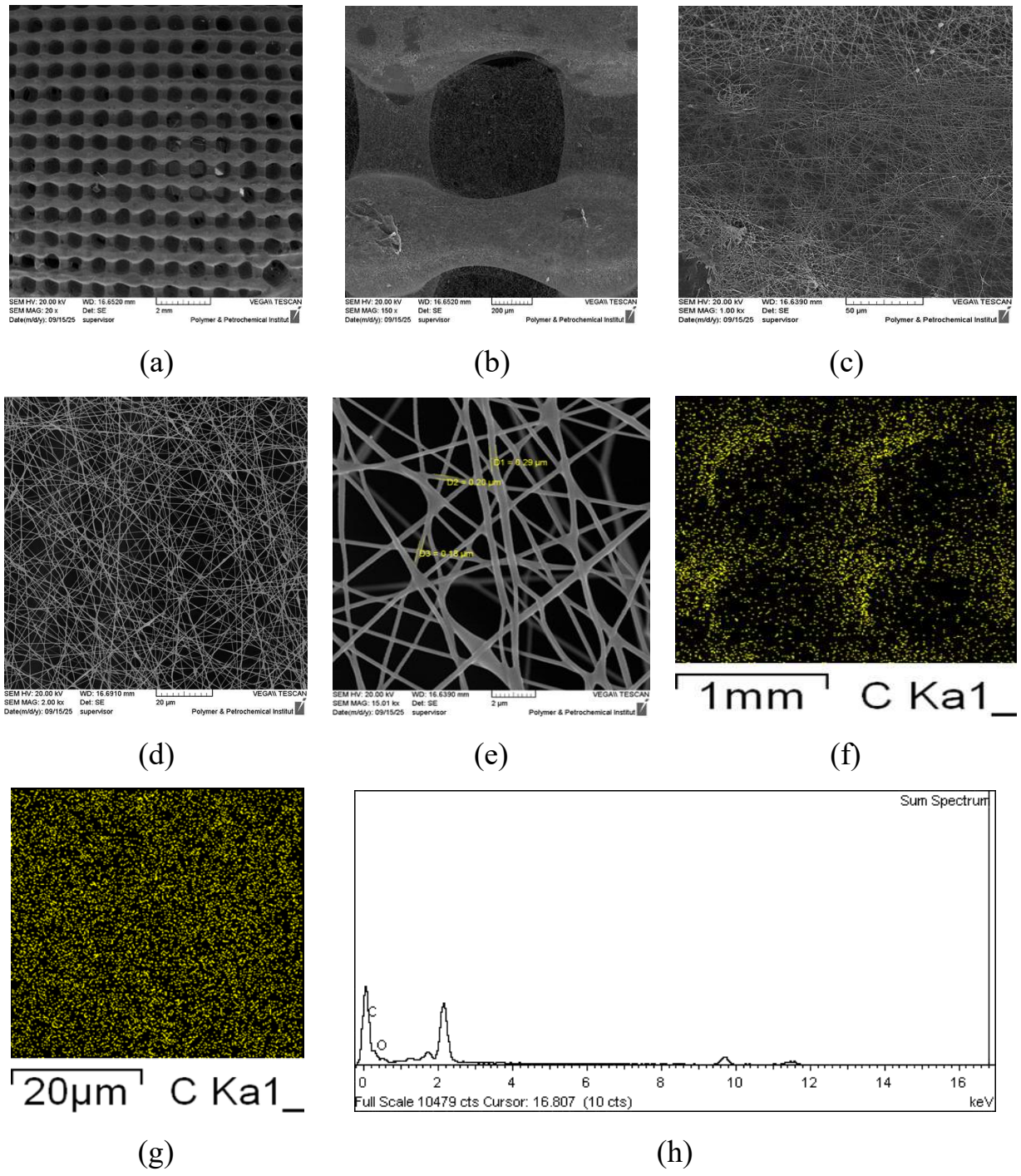

Figure 3. SEM micrographs and EDX analysis of the hybrid scaffold composed of a 3D-printed PCL substrate coated with a crosslinked SA/PVA nanofibrous layer: (a) overall scaffold architecture; (b) nanofibrous layer deposited on scaffold filaments; (c) higher-magnification view of the electrospun network; (d) scaffold–pore interface; (e) representative fiber diameter measurements; (f) cumulative EDX spectrum acquired from the overall scaffold surface; and (g,h) localized EDX analysis of the electrospun nanofibrous layer.

Quantitative analysis showed carbon and oxygen contents of 65.92 wt% and 34.08 wt%, respectively, with no additional elemental signals detected within the analyzed region. To evaluate the composition of the electrospun layer independently from the printed substrate, localized EDX analysis was performed directly on the nanofibrous region at higher magnification (Fig. 3g,h). The localized spectrum similarly showed carbon and oxygen as the predominant elements, while the relative increase in carbon content compared with the cumulative spectrum may be attributed to the polymer-rich nature of the electrospun coating. These findings confirm the deposition of a chemically consistent nanofibrous layer onto the 3D-printed scaffold.

Overall, SEM and EDX analyses confirmed the formation of a structurally integrated hybrid scaffold consisting of a well-defined microporous PCL framework and a continuous electrospun nanofibrous coating.

Morphological and Elemental Analysis of the Aloe vera-Containing Hybrid Scaffold (PCL + SA/PVA/Aloe vera/CA)

The morphology and surface microstructure of the Aloe vera-containing hybrid scaffold were investigated using SEM to evaluate the influence of the bioactive phase on fiber formation and scaffold architecture. SEM observations demonstrated that incorporation of Aloe vera did not disrupt the overall geometry of the 3D-printed PCL substrate. The scaffold preserved its regular interconnected porous architecture, continuous filament arrangement, and open pore structure (Fig. 4a). Following electrospinning, a continuous nanofibrous layer was deposited across both the scaffold filaments and pore regions, indicating stable fiber formation and effective surface coverage.

Higher-magnification images revealed that the electrospun fibers formed an interconnected network over the pore regions and along the scaffold surfaces (Fig. 4b–d). The fibrous layer

bridged adjacent filaments while maintaining pore openness, suggesting that incorporation of Aloe vera did not visibly compromise deposition stability or pore interconnectivity. In some localized regions, increased fiber accumulation was observed, which was likely associated with multilayer deposition during electrospinning. Overall, the nanofibrous coating remained morphologically continuous and structurally integrated with the printed scaffold.

To quantitatively assess fiber morphology, fiber diameter measurements were performed in representative pore regions of the scaffold. The measured fiber diameters were 0.20, 0.17, and 0.17 μm, yielding an average diameter of 0.18 ± 0.02 μm (Fig. 4e). Compared with the base scaffold group, incorporation of Aloe vera resulted in a slight reduction in average fiber diameter while preserving overall fiber uniformity. This observation suggests that Aloe vera influenced the electrospinning behavior of the polymer solution without compromising nanofiber continuity [25].

The elemental composition of the Aloe vera-containing scaffold was further examined using EDX analysis. The cumulative EDX spectrum obtained from the overall scaffold surface, including both the 3D-printed substrate and electrospun layer, demonstrated carbon and oxygen as the dominant elements (Fig. 4g), consistent with the polymeric composition of the scaffold system. Quantitative analysis revealed elemental contents of 66.05 wt% carbon and 33.95 wt% oxygen. To reduce the averaging contribution from the PCL substrate, localized EDX analysis was additionally performed on the electrospun fibrous layer at higher magnification (Fig. 4h). The localized spectrum similarly showed carbon and oxygen as the predominant elements, with slightly increased carbon content relative to the cumulative spectrum, reflecting the polymer-rich composition of the nanofibrous network. No additional elemental signals were detected within the analyzed region.

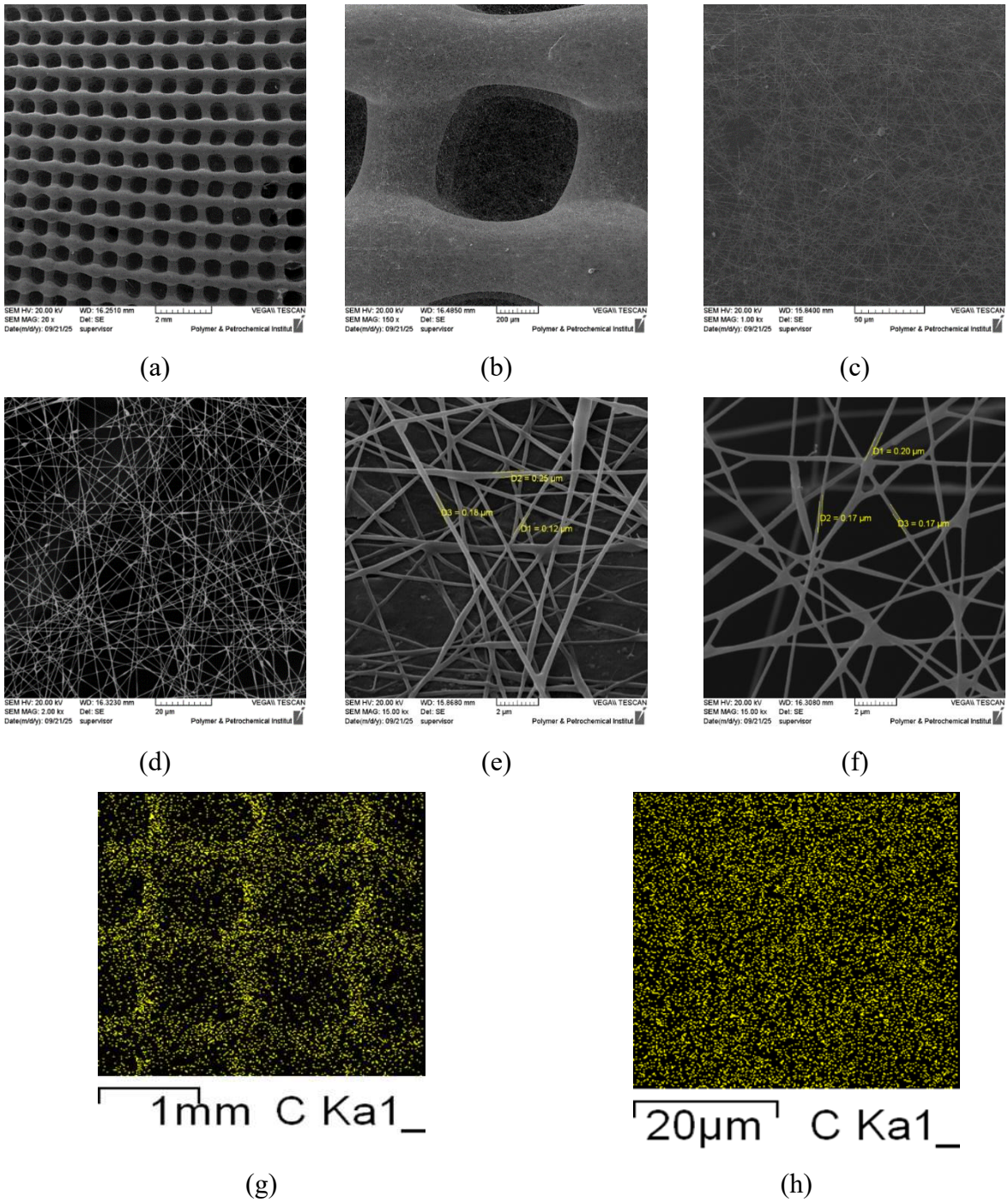

Figure 4. SEM micrographs and EDX analysis of the hybrid scaffold containing Aloe vera: (a) overall scaffold architecture; (b) electrospun nanofibrous network over pore regions; (c) fibers deposited on scaffold filaments; (d) scaffold–pore interface; (e) representative fiber diameter measurements within pore regions; (f) higher-magnification view of the fiber-covered scaffold surface; (g) cumulative EDX spectrum acquired from the overall scaffold surface; and (h) localized EDX analysis of the electrospun nanofibrous layer.

Overall, SEM and EDX analyses confirmed that incorporation of Aloe vera preserved the structural integrity of the hybrid scaffold while slightly modifying fiber morphology. The scaffold maintained continuous nanofiber coverage, open interconnected porosity, and chemically consistent surface composition, supporting the integration of the bioactive phase within the electrospun layer.

Morphological and Elemental Analysis of the Hybrid Scaffold with Ciprofloxacin Incorporated into the Aloe vera Phase (PCL + SA/PVA/Aloe vera+CIP/CA)

The morphology of hybrid scaffolds containing both Aloe vera and ciprofloxacin was investigated using SEM to evaluate the effect of drug incorporation on scaffold architecture and nanofiber organization. SEM overview images demonstrated that the macroscopic geometry of the 3D-printed PCL scaffold remained preserved following drug incorporation (Fig. 5a). The scaffold maintained its interconnected porous network and continuous filament arrangement, although slight rounding of filament edges and less-defined pore boundaries were observed in some regions. Despite these localized variations, the overall scaffold integrity and pore interconnectivity remained intact.

At higher magnifications, the electrospun layer appeared as a continuous and randomly distributed nanofibrous network covering both pore regions and scaffold filaments (Fig. 5b–d). The fibers bridged adjacent pore openings and formed a relatively homogeneous coating across the scaffold surface. In several localized regions, increased fiber accumulation and variations in fiber density were observed, suggesting that incorporation of Aloe vera and ciprofloxacin influenced electrospinning behavior and fiber deposition characteristics [26]. Nevertheless, continuous network formation was maintained throughout the scaffold surface.

Quantitative analysis of fiber diameters within pore regions yielded values of 0.14, 0.18, and 0.13 μm, corresponding to an average fiber diameter of 0.15 ± 0.03 μm (Fig. 5e). Compared with the Aloe vera-containing scaffold without drug loading, the ciprofloxacin-loaded system exhibited slightly thinner fibers, indicating that drug incorporation altered solution properties involved in jet stretching and fiber formation during electrospinning [27]. However, the overall submicron fiber morphology and structural continuity were preserved.

Complementary EDX analysis confirmed the incorporation of ciprofloxacin within the scaffold system. The cumulative EDX spectrum obtained from regions containing both the printed scaffold and electrospun layer revealed carbon, oxygen, and nitrogen as the dominant elements (Fig. 5f–h). The presence of nitrogen, which was not detected in the drug-free scaffold groups, is consistent with the chemical structure of ciprofloxacin and provides evidence of drug incorporation within the scaffold system [28]. Localized EDX analysis performed directly on fiber-rich regions further detected nitrogen within the electrospun layer, indicating that the nanofibrous network served as the primary carrier phase for the loaded drug. Overall, these findings demonstrate that incorporation of ciprofloxacin into the Aloe vera-containing system altered the microstructural organization and surface composition of the electrospun layer without disrupting the macroscopic scaffold architecture.

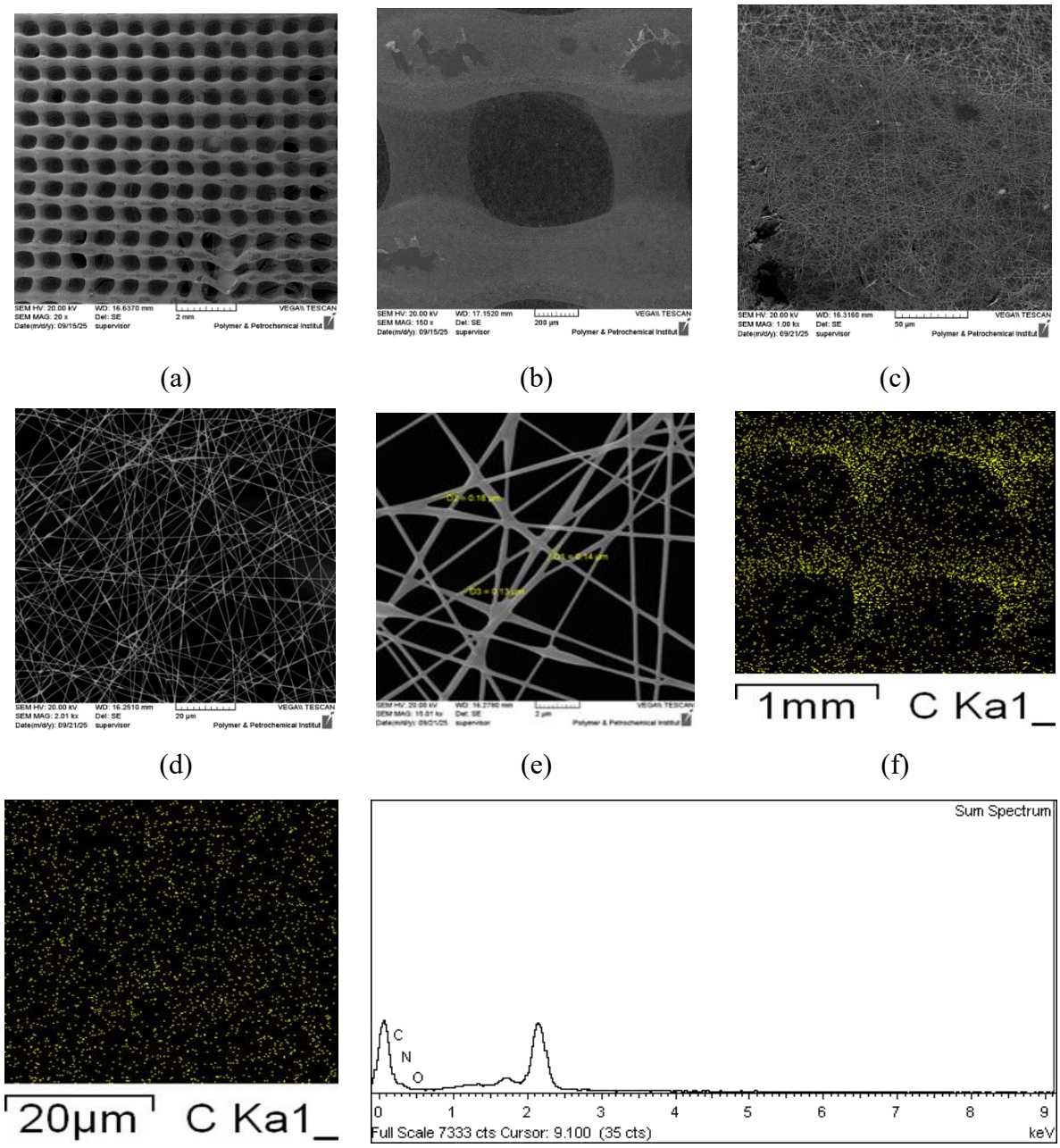

Figure 5. SEM micrographs and EDX analysis of the Aloe vera-containing hybrid scaffold with ciprofloxacin incorporated into the Aloe vera phase: (a) overall scaffold architecture; (b) electrospun nanofibrous layer on the scaffold surface; (c) fibers spanning scaffold regions and pore openings; (d) scaffold–pore interface; (e) representative fiber diameter measurements; (f)

cumulative EDX analysis of the scaffold surface; (g) higher-magnification image of the electrospun layer; and (h) localized EDX spectrum acquired from the fibrous region.

Morphological and Elemental Analysis of the Hybrid Scaffold with Ciprofloxacin Incorporated into the PVA Phase (PCL/SA/PVA+CIP/Aloe vera/CA)

SEM analysis of scaffolds containing ciprofloxacin incorporated directly into the PVA phase demonstrated that the overall architecture of the 3D-printed PCL substrate remained unchanged (Fig. 6a). The scaffold preserved its regular filament arrangement, interconnected pore structure, and open macroporous geometry, indicating that modification of the electrospinning solution did not affect the structural integrity of the printed framework. Pore-focused images further confirmed that pore geometry and scaffold continuity were maintained following electrospinning (Fig. 6b). Higher-magnification SEM images revealed the formation of a continuous electrospun nanofibrous network uniformly distributed across both scaffold filaments and pore regions (Fig. 6c,d). The fibers exhibited random orientation and homogeneous surface coverage, although localized regions of increased fiber density were observed. Compared with the previous scaffold group, variations in local fiber arrangement appeared more pronounced, suggesting that direct incorporation of ciprofloxacin into the PVA phase influenced electrospinning behavior and fiber deposition characteristics [29].

Fiber diameter measurements performed in representative pore regions showed submicron fibers with an average diameter of 0.14 ± 0.06 μm (Fig. 6e), representing the smallest average fiber diameter among the investigated scaffold groups. Although the overall fiber morphology remained continuous, the increased standard deviation indicated greater heterogeneity in fiber distribution and local accumulation. These findings suggest that the location of drug incorporation within the polymer matrix influences electrospinning behavior and nanofiber organization.

EDX analysis further confirmed the presence of ciprofloxacin within the electrospun layer. The cumulative spectrum acquired from regions containing both the PCL substrate and electrospun coating showed carbon, oxygen, and nitrogen as the predominant elements (Fig. 6f–h). Detection of nitrogen is consistent with the nitrogen-containing structure of ciprofloxacin and provides evidence of drug incorporation within the scaffold system. To reduce the averaging effect of the printed substrate, localized EDX analysis was performed directly on fiber-rich regions at higher magnification. The localized spectrum showed an increased relative nitrogen content compared with the cumulative analysis, indicating that the drug was preferentially associated with the electrospun nanofibrous layer. No additional elemental signals were detected within the analyzed region.

Overall, SEM and EDX analyses demonstrated that incorporation of ciprofloxacin within the PVA phase primarily influenced fiber morphology and local heterogeneity of the electrospun layer while preserving the macroscopic architecture of the scaffold. These findings further highlight the importance of drug-loading location in modulating nanofiber morphology and surface composition within multicomponent hybrid scaffold systems.

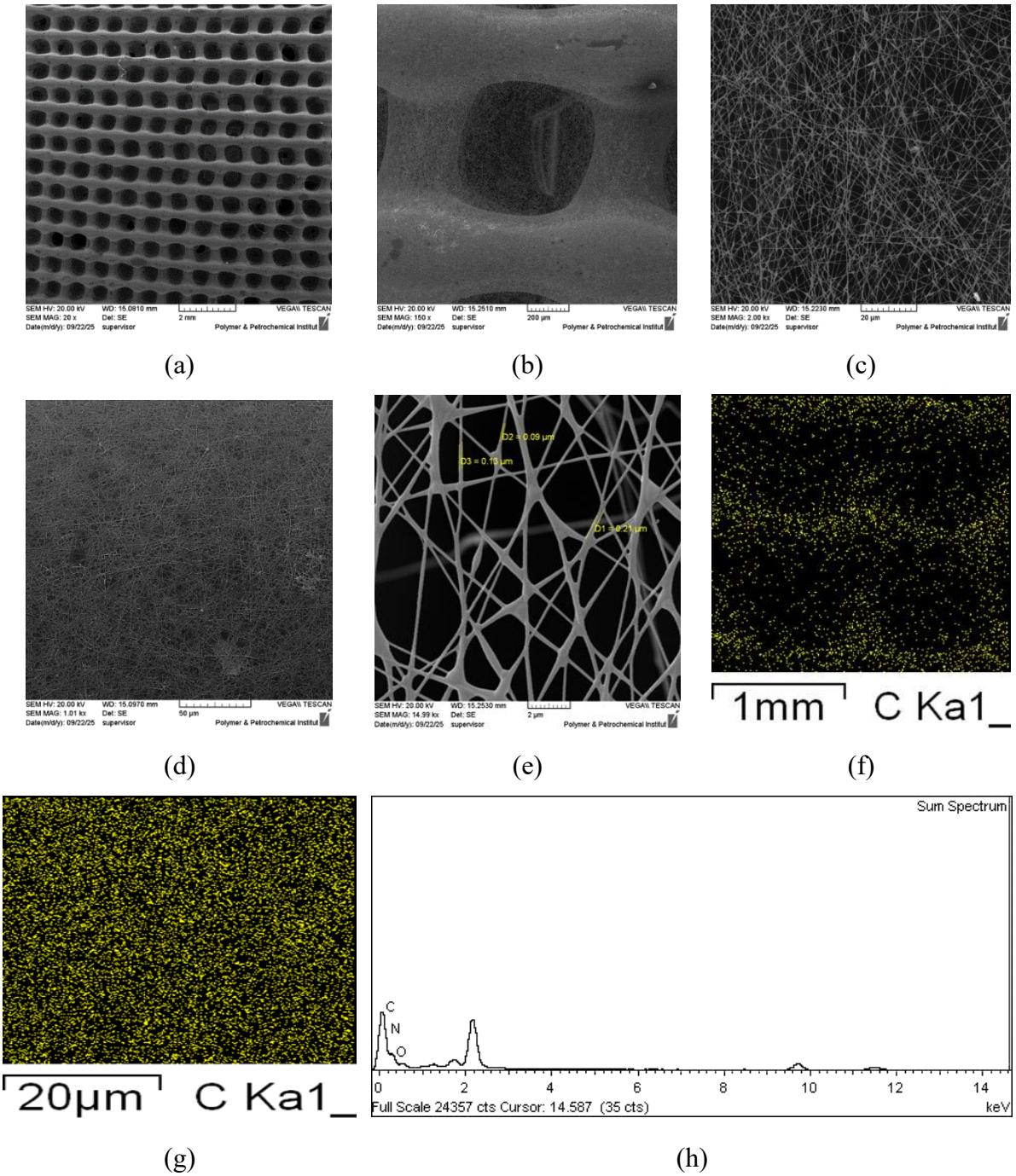

Figure 6. SEM micrographs and EDX analysis of the hybrid scaffold with ciprofloxacin incorporated into the PVA phase: (a) overall scaffold architecture; (b) pore-region morphology and scaffold continuity; (c) electrospun fibers distributed on scaffold filaments; (d) scaffold–pore interface; (e) representative fiber diameter measurements; (f) cumulative

EDX analysis of the scaffold surface; (g) higher-magnification image of the electrospun fibrous layer; and (h) localized EDX spectrum acquired from the nanofibrous region.

Comparative Analysis of Fiber Morphology and Elemental Composition

Comparative analysis of the scaffold groups demonstrated that incorporation of Aloe vera slightly reduced the average fiber diameter while preserving nanofiber uniformity, likely due to changes in solution properties and electrospinning behavior during fiber formation [30]. Incorporation of ciprofloxacin further modified fiber morphology; however, the extent of these changes depended strongly on the drug-loading location. Drug incorporation within the Aloe vera-containing phase produced relatively uniform thin fibers, whereas loading within the PVA phase resulted in the smallest average fiber diameter but increased local heterogeneity and broader fiber size distribution.

EDX analysis showed that drug-free scaffold groups were dominated by carbon and oxygen, reflecting the polymeric composition of the scaffold system. In contrast, ciprofloxacin-loaded groups exhibited detectable nitrogen signals, providing evidence of drug incorporation within the electrospun layer. The relative increase in nitrogen content in localized fiber analyses further demonstrated that the electrospun network functioned as the primary drug-hosting region within the hybrid scaffold.

Together, the combined SEM and EDX results demonstrate that scaffold composition and drug-loading strategy are the primary factors governing nanofiber morphology and surface elemental distribution, while the 3D-printed PCL substrate provides a well-defined structural framework with minimal contribution to microstructural variability.

Table 1. Summary of average fiber diameters and elemental composition of the investigated scaffold groups.

No.	Sample	Fiber Diameter (μm)	Standard Deviation (μm)	Carbon (wt%)	Oxygen (wt%)	Nitrogen (wt%)
1	PCL + SA/PVA/CA	0.22	0.06	65.92	34.08	—
2	PCL + SA/PVA/Aloe vera/CA	0.18	0.02	41.45	22.65	35.90
3	PCL + SA/PVA/Aloe vera+CIP/CA	0.15	0.03	66.05	33.95	—
4	PCL + SA/PVA+CIP/Aloe vera/CA	0.14	0.06	47.31	28.73	23.95

FTIR Analysis of Hybrid Scaffolds

FTIR spectroscopy was employed to investigate the chemical structure of the developed hybrid scaffolds and to evaluate compositional variations induced by Aloe vera incorporation and ciprofloxacin loading (Fig. 7). It should be noted that the recorded spectra represent the entire hybrid system, including the 3D-printed PCL substrate and the electrospun polymeric layer; therefore, several characteristic bands, particularly in the carbonyl region, may arise from overlapping contributions of PCL, esterified crosslinked networks, and other polymeric components. Accordingly, comparative analysis across groups was prioritized.

The base scaffold exhibited a broad absorption band at 3600–3000 cm^{-1} corresponding to O–H stretching vibrations, reflecting the presence of abundant hydroxyl groups within the polymeric network [31]. The band observed at 1750–1650 cm^{-1} was attributed to carbonyl (C=O) stretching associated with PCL and ester linkages formed during crosslinking [32, 33]. Additionally, the region between 1250–950 cm^{-1}, assigned to C–O and C–O–C vibrations [34], confirmed the

integrity of the polysaccharide-based network and successful formation of the blended polymer structure (Fig. 7a).

Following Aloe vera incorporation, a noticeable increase in the intensity and breadth of the O–H stretching band was observed, indicating an increased density of hydroxyl-containing functional groups within the scaffold matrix [35]. In addition, subtle variations in the 1650–1400 cm^{-1} region, associated with carboxylate ($–COO^–$) vibrations [36], were detected. Following Aloe vera incorporation, a noticeable increase in the intensity and breadth of the O–H stretching band was observed, indicating an increased density of hydroxyl-containing functional groups within the scaffold matrix [35]. In addition, subtle variations in the 1650–1400 cm^{-1} region, associated with carboxylate ($–COO^–$) vibrations [36], were detected. These observed spectral changes further supported the successful incorporation of Aloe vera and enhanced hydrogen-bonding interactions within the polymer network (Fig. 7b) [37].

In scaffolds loaded with ciprofloxacin within the Aloe vera-containing system, a relative decrease in O–H band intensity was observed alongside subtle changes in the fingerprint region (1250–950 cm^{-1}). These variations may indicate non-covalent interactions, such as hydrogen bonding, between ciprofloxacin and the polymer matrix [38], without evidence of structural disruption in the overall network (Fig. 7c) [39] .

When ciprofloxacin was incorporated directly into the PVA phase, the FTIR spectrum showed a more homogeneous distribution of characteristic bands, with no emergence of new distinct peaks. The absence of distinct drug-related bands suggests homogeneous distribution of ciprofloxacin within the polymeric matrix with no evidence of phase separation detectable by FTIR analysis (Fig. 7d) [26].

Overall, comparative FTIR analysis indicates that scaffold chemical signatures are primarily influenced by the incorporation of Aloe vera and the localization strategy of ciprofloxacin. Aloe vera contributes to an increase in hydroxyl-associated functional groups, while ciprofloxacin induces subtle, site-dependent modifications in hydrogen-bonding interactions within the polymeric network. The characteristic absorption bands of the PCL substrate remained consistent across all groups, confirming that the observed spectral variations predominantly originate from modifications in the electrospun polymeric layer.

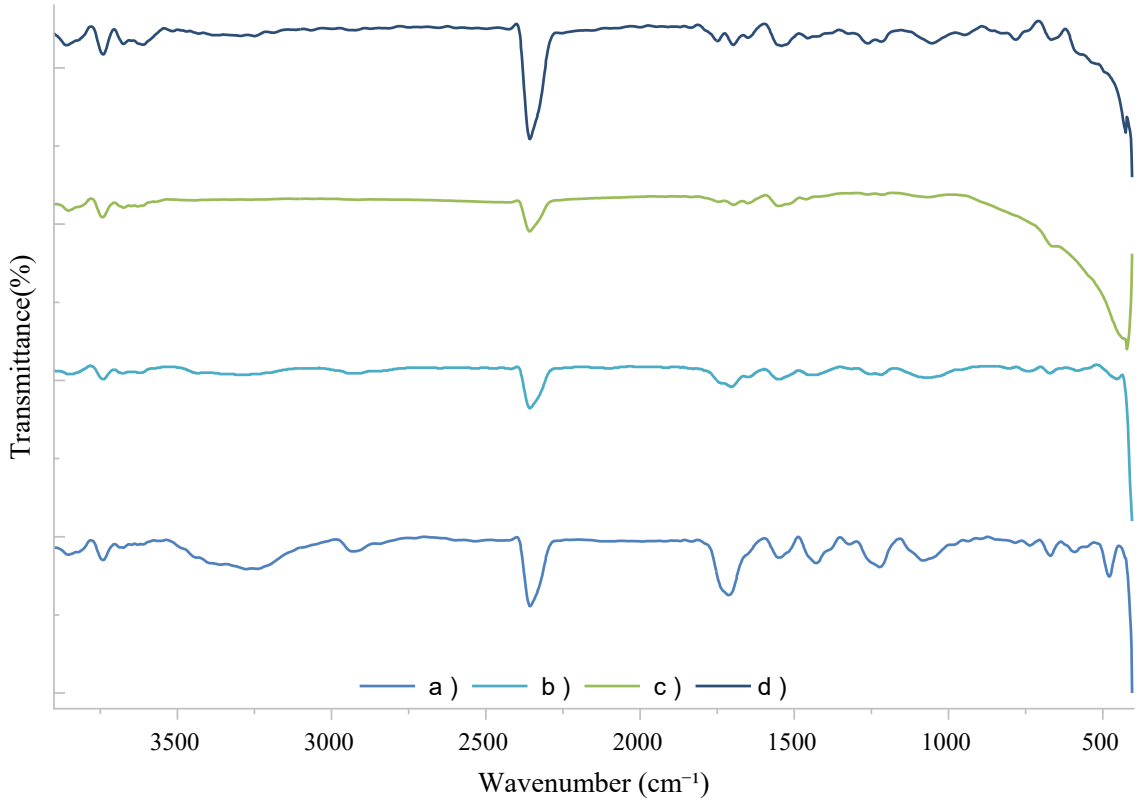

Figure 7. FTIR spectra of: (a) PVA/SA, (b) PVA/SA/Aloe vera, (c) PCL + PVA/SA/Aloe vera + CIP, and (d) PCL + PVA + CIP/SA/Aloe vera system.

Thermal Analysis of Hybrid Scaffolds

Thermogravimetric Analysis (TGA)

TGA was performed to evaluate the thermal stability and degradation behavior of the hybrid scaffolds (Fig. 8). Since all formulations incorporated a 3D-printed PCL substrate, the observed thermal responses were interpreted on a comparative basis, with variations primarily attributed to modifications in the polymeric surface layer rather than the structural backbone.

All samples exhibited a characteristic multi-step degradation profile, indicating overlapping decomposition mechanisms within the multicomponent system. In the initial stage (up to ~150 °C), negligible mass loss (<0.3%) was observed, corresponding to the removal of physically adsorbed moisture associated with hydrophilic functional groups present in the SA/PVA matrix, confirming effective drying of the samples [40].

A gradual mass loss in the intermediate region (~200–250 °C) was attributed to the onset of polymer destabilization and internal dehydration processes. The relatively smooth transition suggests that citric acid-mediated crosslinking enhances thermal resistance by delaying abrupt structural breakdown[16].

The main degradation stage occurred between approximately 250 and 400 °C, where the majority of mass loss was recorded. This region corresponds to overlapping degradation of the polymeric constituents, including PVA, SA, and partial contribution of PCL, along with decomposition of crosslinked networks and incorporated bioactive/pharmaceutical agents. The complex overlapping behavior reflects the multicomponent nature of the system, limiting the resolution of individual contributions via TGA alone. DTG analysis indicated maximum degradation rates in the range of ~360–375 °C, corresponding to dominant chain-scission events.

At temperatures above 400 °C, gradual mass loss was attributed to carbonization and formation of thermally stable residues. The final residual mass (~10–11%) indicates the presence of stable carbonaceous structures derived from the polymeric network.

Comparative analysis revealed that Aloe vera incorporation broadened the degradation profile, indicating increased thermal heterogeneity without compromising overall stability. Ciprofloxacin loading induced minor shifts in degradation kinetics, reflected in subtle variations in DTG peak temperatures, without altering the overall degradation pathway or causing premature decomposition. Overall, the thermal stability of the hybrid system is primarily governed by the crosslinked PVA/SA matrix, while additives modulate degradation kinetics. The PCL substrate served as a common structural component across all formulations, allowing comparative evaluation of the effects of scaffold composition on thermal behavior.

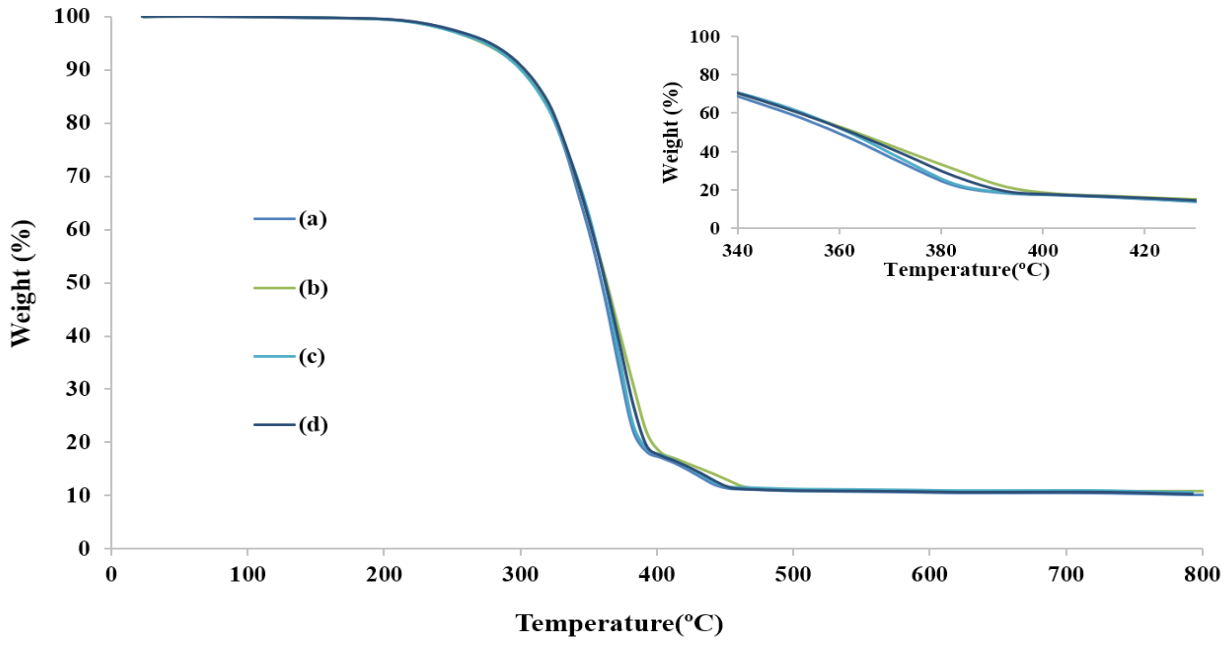

Figure 8. TGA curves of hybrid scaffolds: (a) PVA/SA (b) PVA/SA/Aloe vera (c) PCL + PVA/SA/Aloe vera + CIP (d) PCL + PVA + CIP /SA/Aloe vera

Table 2. Thermogravimetric parameters of hybrid scaffold systems, including residual mass, final degradation temperature, maximum mass loss rate, DTG peak temperature, and characteristic weight-loss temperatures (T_5% and T_{10}%). Data are reported for comparative evaluation of thermal behavior across formulations.

Composition	Residual Mass (%)	Maximum Mass Loss Rate (%/min)	DTG Peak Temperature (°C)	T_{10}% (°C)	T_5% (°C)
PCL + SA/PVA/CA	10.10	–12.78	372.72	302.11	277.12
PCL + SA/PVA/Aloe Vera	10.62	–13.75	372.66	300.27	274.35
PCL + SA/PVA/Aloe Vera + CIP	10.76	–9.85	362.72	301.06	273.23
PCL + SA/PVA+ CIP/Aloe Vera	10.26	–11.57	372.71	303.25	277.63

Derivative Thermogravimetric Analysis (DTG)

DTG analysis was performed to further investigate the degradation kinetics of the hybrid scaffolds during the principal decomposition stage (Fig. 9). Because all formulations contained the same PCL substrate, the observed DTG responses were interpreted comparatively, with differences primarily attributed to variations in the composition of the electrospun layer. The recorded DTG curves exhibited a dominant degradation peak in the temperature range of approximately 362–373 °C, corresponding to the main decomposition stage of the polymeric network. This thermal event is associated with overlapping degradation processes involving PVA, SA, citric acid-mediated crosslinked structures, and the incorporated bioactive components [16, 41].

Above ~400 °C, the degradation rate decreased significantly, indicating a transition toward carbonization. At ~800 °C, a residual mass of ~10% was observed, attributed to carbonaceous char and thermally stable residues. This result establishes a thermal baseline for evaluating the effect of bioactive and pharmaceutical additives.

The drug-free scaffold exhibited a DTG peak at approximately 372–373 °C with a maximum degradation rate of about –12.8 to –13.7% min^{-1}, establishing the thermal baseline of the hybrid system. Incorporation of Aloe vera did not significantly alter the peak temperature, indicating that the primary degradation mechanism remained governed by the crosslinked PVA/SA network. However, a broader DTG profile was observed, suggesting increased heterogeneity in degradation pathways due to the presence of Aloe vera and its polysaccharide-rich composition [42].

The residual mass (~10.6–10.9% at ~800 °C) remained comparable to the base scaffold, confirming that Aloe vera incorporation does not compromise thermal stability. Scaffolds containing ciprofloxacin exhibited slight modifications in degradation behavior. In particular, the formulation containing ciprofloxacin within the Aloe vera phase showed a modest reduction in DTG peak temperature and maximum degradation rate. These changes may be attributed to drug–polymer interactions, including hydrogen bonding and altered segmental mobility within the polymer matrix [43].

Nevertheless, the overall degradation pathway remained comparable to that of the drug-free scaffold, indicating that ciprofloxacin incorporation did not fundamentally alter the thermal decomposition mechanism of the hybrid system.

For all scaffold formulations, the degradation rate decreased markedly above approximately 400 °C, indicating transition to the carbonization stage and formation of thermally stable carbonaceous residues. The residual mass remained within a narrow range of approximately 10–11%,

demonstrating that incorporation of Aloe vera and ciprofloxacin only slightly influenced degradation kinetics without significantly affecting the overall thermal stability of the scaffolds. Overall, DTG analysis confirmed that the principal degradation mechanism was dominated by decomposition of the crosslinked polymeric network, while incorporation of bioactive and pharmaceutical components produced only minor variations in degradation kinetics and peak characteristics.

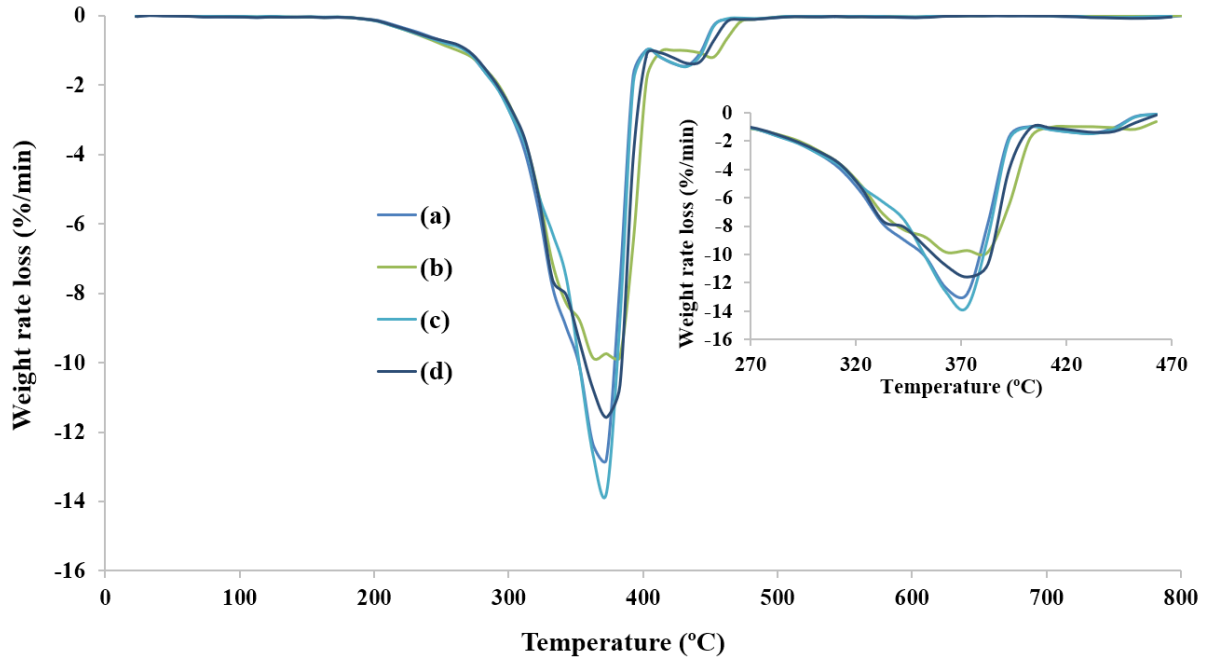

Figure 9. DTG curves of hybrid scaffolds: (a) PVA/SA (b) PVA/SA/Aloe vera (c) PCL + PVA/SA/Aloe vera + CIP (d) PCL + PVA + CIP /SA/Aloe vera

Comparative Evaluation of Thermal Behavior

The thermal behavior of the hybrid scaffold formulations was comparatively evaluated based on the TGA and DTG results presented in Table 2 and Figures 8 and 9. All scaffold groups exhibited a similar multistep degradation profile, indicating that the overall thermal response was primarily

governed by the crosslinked PVA/SA matrix together with the common PCL structural framework.

In all formulations, negligible mass loss was observed below approximately 150 °C, corresponding to the removal of physically adsorbed moisture. The principal degradation stage occurred between approximately 250 and 400 °C, where the majority of mass loss was recorded. This degradation region was associated with the overlapping decomposition of the polymeric network, including degradation of PVA chains, sodium alginate backbones, and citric acid-mediated ester crosslinks.

Comparative DTG analysis revealed dominant degradation peaks within the range of 362–373 °C. The base hybrid scaffold and the Aloe vera-containing scaffold exhibited nearly identical DTG peak temperatures (372.72 and 372.66 °C, respectively), indicating that incorporation of Aloe vera did not significantly alter the primary degradation mechanism. In contrast, the scaffold containing ciprofloxacin incorporated into the Aloe vera phase showed a slight reduction in DTG peak temperature (362.72 °C) together with a lower maximum degradation rate, suggesting minor modifications in degradation kinetics arising from interactions between the drug and the polymeric matrix. The scaffold containing ciprofloxacin incorporated into the PVA phase exhibited a DTG peak temperature (372.71 °C) comparable to that of the base formulation, indicating preservation of the overall degradation behavior.

At temperatures above approximately 400 °C, all scaffold groups entered a gradual carbonization stage characterized by a progressive decrease in degradation rate and formation of thermally stable residues. Residual mass values remained within a narrow range of 10.10–10.76%, demonstrating that incorporation of Aloe vera and ciprofloxacin did not substantially affect the final thermal stability of the scaffold system.

Overall, the TGA and DTG results indicate that incorporation of Aloe vera and ciprofloxacin slightly influenced degradation kinetics without significantly altering the fundamental thermal degradation pathway of the hybrid scaffolds. The comparable values of T_5%, T_{10}%, DTG peak temperature, maximum degradation rate, and residual mass further confirm that the thermal stability of the developed scaffolds was predominantly governed by the crosslinked polymeric network, while the incorporated bioactive and pharmaceutical components produced only minor variations in thermal behavior. [44].

Biological Evaluation of Hybrid Scaffolds

Cell Viability Assessment by Tetrazolium-Based Assay

The biological response of the developed hybrid scaffolds was evaluated using a tetrazolium salt–based colorimetric assay, which assesses cellular metabolic activity through reduction of tetrazolium salts to formazan products [45]. Since metabolic activity is closely associated with viable cellular function, this assay enables comparative evaluation of scaffold-induced cellular responses over time. Measurements were conducted on the complete hybrid systems, including both the 3D-printed PCL substrate and the electrospun polymeric nanofibrous layers; therefore, the obtained responses reflect the combined influence of scaffold architecture, surface chemistry, and drug incorporation strategy.

To minimize inter-experimental variability, optical density values measured at 570 nm were normalized against the negative control (cells cultured in the absence of scaffolds), and results were expressed as relative cell viability percentages (mean ± SD, n = 3). Blank absorbance values were subtracted prior to normalization. Because the assay primarily reflects cellular metabolic activity rather than direct cell number, observed variations may represent changes in metabolic state in addition to alterations in proliferation or cytotoxic response [46].

Following 12 h of incubation, all scaffold formulations maintained relative viability values above 60% compared with the negative control, indicating moderate to acceptable early cytocompatibility, although viability values varied among formulations and remained close to commonly accepted in vitro cytotoxicity thresholds [47].

Among the tested formulations, the ciprofloxacin-loaded scaffold containing drug incorporation within the PVA phase (PCL + PVA + CIP /SA/Aloe vera) exhibited the highest metabolic activity, suggesting that the initial cellular response was not significantly affected by ciprofloxacin incorporation. The drug-free scaffold (PVA/SA/Aloe vera) also demonstrated relatively high viability, supporting the intrinsic cytocompatibility of the crosslinked SA/PVA/CA/Aloe vera matrix and indicating favorable early cell–material interactions.

In contrast, the scaffold containing ciprofloxacin within the Aloe vera phase (PCL + PVA/SA/Aloe vera + CIP) exhibited comparatively lower viability at this time point, although the values remained above commonly accepted cytotoxicity thresholds. This reduction may be associated with a higher initial local exposure to ciprofloxacin during the early stage of incubation, leading to transient modulation of cellular metabolism during early exposure [48].

Overall, the 12 h results demonstrate that all scaffold formulations provide an acceptable biological environment during the initial stages of cell–scaffold interaction, while suggesting a potential influence of drug localization on early cellular metabolic activity.

After 48 h of incubation, all scaffold groups maintained viability levels above 58% relative to the negative control, indicating sustained cellular metabolic activity during prolonged exposure. The PCL + PVA + CIP/SA/Aloe vera scaffold exhibited a moderate reduction in viability relative to the 12 h time point, which may reflect cumulative exposure to ciprofloxacin and gradual modulation of cellular metabolic activity over time. In contrast, the drug-free PVA/SA/Aloe vera

scaffold maintained a relatively stable viability profile, further supporting the inherent cytocompatibility of the polymeric matrix.

Interestingly, the PCL + PVA/SA/Aloe vera + CIP scaffold demonstrated improved viability compared with its early-stage response. This observation may indicate progressive cellular adaptation to the scaffold environment and reduced influence of the initial drug exposure. These findings collectively suggest that cellular behavior is time-dependent and may be influenced by the localization of ciprofloxacin within the polymeric matrix [49].

Following 72 h of incubation, distinct differences in cell viability were observed among the scaffold formulations, reflecting cumulative scaffold–cell interactions during extended exposure. The PCL + PVA + CIP/SA/Aloe vera scaffold showed a further decrease in metabolic activity relative to earlier time points, potentially associated with prolonged exposure to the scaffold environment and the presence of ciprofloxacin. However, considering the metabolic basis of the assay, this reduction should not be interpreted exclusively as definitive cytotoxicity, since metabolic suppression may occur independently of irreversible cell death.

The drug-free PVA/SA/Aloe vera scaffold continued to maintain moderate viability throughout the incubation period, indicating stable long-term compatibility between the cells and the base polymeric network.

Notably, the PCL + PVA/SA/Aloe vera + CIP scaffold exhibited the highest relative viability after 72 h. This observation suggests improved cellular adaptation during prolonged exposure and indicates that the localization of ciprofloxacin within the scaffold system may influence long-term cellular metabolic activity. The sustained viability observed for this formulation further supports its favorable biological performance under extended culture conditions.

Overall, the biological assessment demonstrates that scaffold composition and drug-localization strategy influence the temporal cellular response of the hybrid systems. While all formulations exhibited moderate to acceptable cytocompatibility, the PCL + PVA/SA/Aloe vera + CIP scaffold showed the most favorable long-term cellular response among the investigated groups. These findings highlight the importance of integrating scaffold architecture, polymer composition, and drug-distribution strategy in the design of multifunctional hybrid scaffolds for bone tissue engineering applications [50].

The tetrazolium salt–based assay demonstrated a time-dependent variation in cellular metabolic activity among the investigated hybrid scaffolds, which was influenced by scaffold composition and ciprofloxacin localization strategy. Although all formulations maintained viability levels within ranges generally considered acceptable for in vitro biomaterial evaluation, differences among the groups indicate that the position of ciprofloxacin incorporation within the polymeric matrix affects the temporal cellular response.

The scaffold containing ciprofloxacin incorporated into the PVA phase (PCL + PVA + CIP/SA/Aloe vera) exhibited the highest metabolic activity during the early incubation period, suggesting limited short-term interference of the released drug with cellular metabolic activity. In contrast, the scaffold containing ciprofloxacin incorporated into the Aloe vera phase (PCL + PVA/SA/Aloe vera + CIP) showed lower initial viability but demonstrated improved cellular response at extended incubation times. This behavior may be associated with differences in drug distribution and release kinetics within the hybrid matrix; however, further correlation with independent drug-release measurements is required to confirm this relationship.

The drug-free scaffold (PVA/SA/Aloe vera) maintained relatively stable viability throughout the incubation period, confirming the favorable cytocompatibility of the crosslinked polymeric network and supporting its suitability as a bioactive scaffold component.

It should be emphasized that the tetrazolium-based assay primarily reflects cellular metabolic activity rather than direct cell number, proliferation rate, or definitive in vivo biocompatibility [46]. Therefore, the obtained results should be interpreted as relative indicators of cellular response under the investigated culture conditions. More comprehensive biological evaluation would require complementary analyses, including live/dead staining, cell morphology assessment, proliferation studies, osteogenic differentiation assays, and correlation with drug-release behavior [51].

Overall, these findings confirm the cytocompatible nature of the developed hybrid scaffolds and demonstrate that both scaffold composition and drug-localization strategy play important roles in regulating time-dependent biological performance. The results further highlight the importance of controlled incorporation of bioactive and pharmaceutical components within multicomponent scaffold systems designed for bone tissue engineering applications.

Table 3. Cell viability percentages of different scaffold formulations after 12 h of incubation, determined using the tetrazolium salt–based colorimetric assay. Optical density values were measured at 570 nm and normalized relative to the negative control (mean ± SD, n = 3).

Replicates (n)	Cell viability (% of negative control)	Optical density at 570 nm (mean ± SD)	Scaffold composition	No.
3	69.45 ± 4.34	0.1440 ± 0.0090	PCL + SA/PVA/Aloe vera/CA	2
3	61.25 ± 1.93	0.1270 ± 0.0040	PCL + SA/PVA/Aloe vera+CIP/CA	3
3	74.12 ± 1.55	0.1537 ± 0.0032	PCL + SA/PVA+CIP/Aloe vera/CA	4
3	100.00	0.2073 ± 0.0162	Cells without scaffold contact (negative control)	Negative control

Notes:

- Blank absorbance values (medium without cells) were subtracted prior to normalization.
- Cell viability percentages were calculated relative to the negative control.
- The assay reflects cellular metabolic activity; therefore, changes in measured values may indicate alterations in metabolic state rather than direct changes in cell number.

Time-Dependent Cellular Response of Hybrid Scaffolds

Comparative analysis of the tetrazolium salt–based cell viability assay at 12, 48, and 72 h demonstrated time-dependent variations in cellular metabolic activity among the developed hybrid scaffolds (Table 4, Fig 10). Since the assay was performed on the complete hybrid constructs, the obtained values represent the integrated biological effect of both the 3D-printed PCL substrate and the overlying electrospun polymeric nanofibrous surface layers. As the PCL backbone was identical in all formulations, the observed intergroup differences are primarily attributed to variations in surface composition and drug incorporation strategy.

The temporal response of the (PCL + PVA + CIP/SA/Aloe vera/CA) scaffold showed a progressive reduction in cell viability from 12 to 72 h.This decline may be associated with

cumulative drug exposure and time-dependent modulation of cellular metabolic activity within the scaffold microenvironment, as drug-release behavior can significantly influence biological responses over prolonged exposure periods [52]. Importantly, because tetrazolium-based assays primarily reflect cellular metabolic activity rather than direct cell death, the observed decrease should not be interpreted as definitive cytotoxicity, but rather as a relative alteration in cellular metabolic status under prolonged exposure conditions [50].

The (PCL + SA/PVA/Aloe vera/CA) scaffold exhibited a relatively stable viability profile throughout the incubation period. This behavior indicates favorable compatibility between the cells and the polymeric matrix under the investigated culture conditions. The relatively stable viability profile suggests that the base polymeric matrix (PCL + PVA/SA/citric acid/Aloe vera) maintains acceptable cytocompatibility throughout the incubation period, consistent with previous reports demonstrating the favorable biocompatibility of PVA/SA-based scaffold systems[23]. Only limited fluctuations in cellular metabolic activity were observed during.

In contrast, the (PCL + SA/PVA/Aloe vera + CIP/CA) scaffold demonstrated a distinct temporal response. Cell viability increased at 48 and 72 h relative to the initial 12 h measurement and exceeded that of the other scaffold groups at later time points. This behavior may indicate progressive cellular adaptation and reduced influence of the initial drug exposure during prolonged incubation [53]. Furthermore, the presence of Aloe vera may contribute to enhanced surface bioactivity and improved long-term cell–material interactions [54]. Nevertheless, mechanistic interpretation of this trend requires complementary correlation with independent drug-release studies and additional biological assays [55].

Overall, the comparative results demonstrate that scaffold biocompatibility is strongly influenced by the interplay between exposure duration, polymeric surface composition, and drug

localization strategy. The observed differences should therefore be interpreted as relative trends in cellular metabolic response rather than absolute indicators of cytotoxicity. Collectively, these findings support the cytocompatible nature of the developed hybrid scaffolds and highlight the importance of integrating physicochemical, biological, and drug-release analyses for comprehensive scaffold evaluation.

Table 4. Time-dependent comparison of cell viability percentages of hybrid scaffolds after 12, 48, and 72 h of incubation based on the tetrazolium salt–based colorimetric assay.

No.	Incubation Time (h)	Scaffold Composition	Optical Density at 570 nm	Cell Viability (% of Negative Control)	Replicates (n)
2	12	PCL + SA/PVA/Aloe vera/CA	0.1440	69.45	3
	48		0.1737	58.80	3
	72		0.1790	52.91	3
3	12	PCL + SA/PVA/ Aloe vera + CIP/CA	0.1270	61.25	3
	48		0.2260	76.52	3
	72		0.2447	72.32	3
4	12	PCL + PVA + CIP/SA/ Aloe vera/CA	0.1537	74.12	3
	48		0.1720	58.24	3
	72		0.1107	32.71	3
Negative Control	—	Cells cultured without scaffold contact	Time-dependent normalization reference	100.00	3

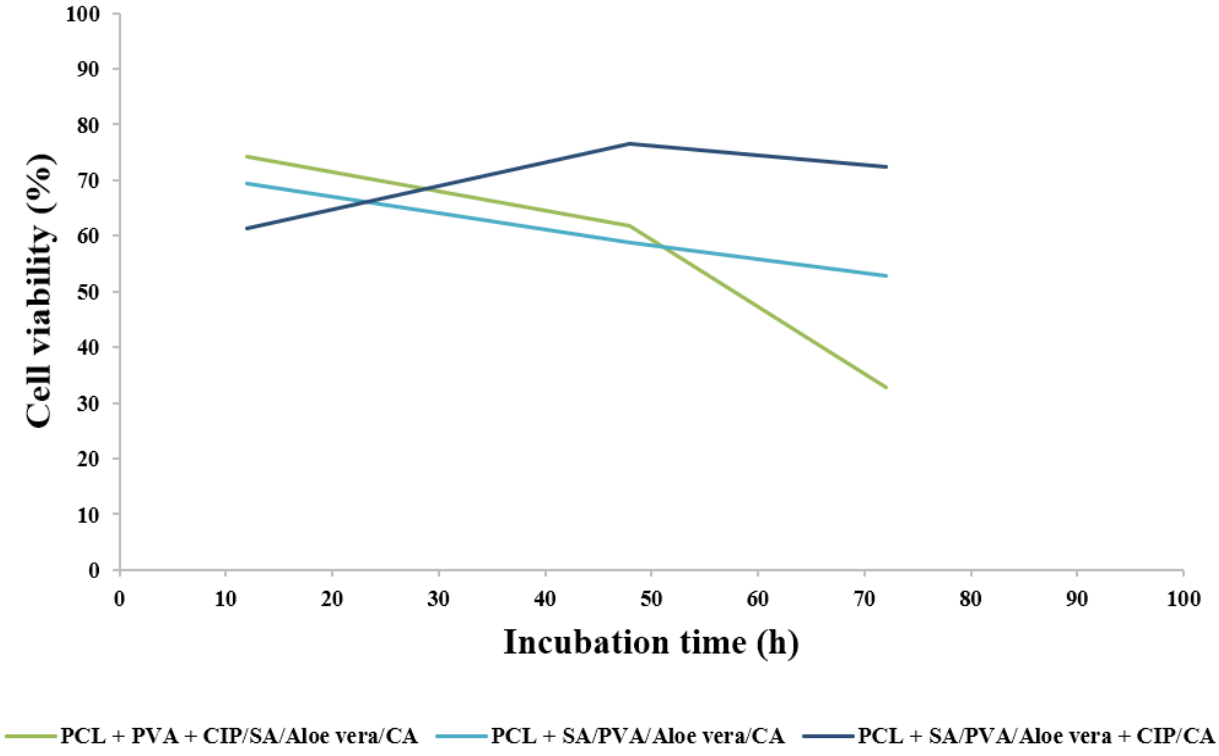

Figure 10. Time-dependent comparison of cell viability percentages of hybrid scaffold systems at 12, 48, and 72 h based on the tetrazolium salt–based metabolic activity assay

Hybrid Scaffold Design and Characterization

In this study, the hybrid scaffold was designed to balance polymer processability with incorporation of bioactive components, enabling formation of a stable nanofibrous network while incorporating sodium alginate, Aloe vera, and ciprofloxacin within the scaffold structure. Electrospinning optimization demonstrated that sodium alginate alone lacked sufficient viscoelasticity to produce continuous fibers [56], whereas increasing alginate content in binary SA/PVA systems progressively induced bead formation and morphological instability [57]. In contrast, the 50/50 SA/PVA ratio provided a suitable balance between alginate bioactivity and

PVA-assisted electrospinnability, yielding a uniform network of continuous fibers. Accordingly, this formulation was selected as the base system for subsequent scaffold modifications.

Morphological analysis of the electrospun coating deposited onto 3D-printed polycaprolactone scaffolds revealed formation of a continuous nanofibrous layer integrated with the macroporous printed substrate, resulting in a hierarchical multiscale architecture composed of interconnected macropores and nanoscale fibers. Fiber diameter measurements showed an average diameter of 0.22 ± 0.06 μm in the base scaffold, which decreased to 0.18 ± 0.02 μm following incorporation of Aloe vera. Further reduction in fiber diameter was observed after ciprofloxacin loading, reaching 0.15 ± 0.03 μm when incorporated through the Aloe vera phase and 0.14 ± 0.06 μm when introduced into the PVA phase. These variations likely reflect additive-induced changes in solution rheology, conductivity, and jet stretching behavior during electrospinning, suggesting that the drug-loading site may influence the final fiber microstructure [58, 59].

Elemental analysis further supported these structural observations. Drug-free scaffolds exhibited only carbon and oxygen signals, whereas ciprofloxacin-containing scaffolds showed detectable nitrogen, supporting the presence of ciprofloxacin within the electrospun layer. Therefore, compositional differences among scaffold groups were reflected not only in morphology but also in relative surface elemental characteristics.

Fourier-transform infrared spectroscopy provided additional insight into relative chemical modifications within the hybrid systems. Incorporation of Aloe vera increased the hydroxyl-related spectral contribution, with the O–H/C=O area ratio reaching 4.046540 in the Aloe vera-containing scaffold without drug loading, suggesting increased contribution of hydroxyl-containing groups and enhanced hydrogen-bonding interactions [60, 61].

Ciprofloxacin incorporation generated more complex spectral behavior depending on the loading strategy. In scaffolds where the drug was incorporated into the PVA phase, the 1250–950 cm^{-1} region—which includes contributions from C–O and C–O–C vibrations of the polymer matrix as well as C–N and C–F bonds associated with ciprofloxacin [62]— showed the highest relative intensity compared with the carbonyl region (2.322515), suggesting a greater contribution of ciprofloxacin-related functional groups within the polymeric matrix. In contrast, scaffolds containing ciprofloxacin within the Aloe vera phase exhibited a relative reduction in hydroxyl intensity accompanied by enhancement of the 1250–950 cm^{-1} region, suggesting intermolecular interactions between the drug and bioactive constituents [63]. Collectively, these findings suggest that drug localization affects the relative chemical environment of the scaffold system and may contribute to variations in fiber morphology observed by SEM.

Thermal analysis further revealed the relationship between scaffold composition and thermal behavior. All formulations exhibited a similar multi-step degradation profile characterized by a principal degradation stage between approximately 250–400 °C and final residual masses near 10%, indicating preservation of the overall thermal degradation mechanism. Nevertheless, quantitative thermal parameters revealed formulation-dependent variations. The Aloe vera/ciprofloxacin-containing scaffold exhibited a lower DTG peak temperature (~362.7 °C) and reduced maximum degradation rate (~−9.85% min^{-1}), whereas the Aloe vera-containing scaffold without drug loading showed the highest degradation rate (~−13.75% min^{-1}). These observations suggest that bioactive and pharmaceutical additives modulate degradation kinetics and thermal stress distribution without causing substantial changes in the overall thermal degradation profile of the hybrid scaffold system [64].

The structural and physicochemical variations observed among the scaffold groups were also reflected in their biological responses. Tetrazolium salt–based cell viability assays revealed a time-dependent variation in cellular metabolic activity associated with scaffold composition and drug-loading strategy. At 12 h, all scaffolds maintained viability values above 60%, including 74.12% for the PCL + PVA + CIP/SA/Aloe vera scaffold, 69.45% for the drug-free PCL + PVA/SA/Aloe vera scaffold, and 61.25% for the PCL + PVA/SA/Aloe vera + CIP scaffold. However, the temporal response profiles diverged during extended incubation. At 48 h, the Aloe vera-associated ciprofloxacin-loaded scaffold exhibited the highest viability (76.52%), whereas the PVA-associated ciprofloxacin-loaded scaffold showed a progressive reduction in metabolic activity. By 72 h, the Aloe vera-associated ciprofloxacin-loaded scaffold maintained relatively high viability (72.32%), while the PVA-associated system decreased to 32.71%. These findings suggest that the localization of ciprofloxacin within the polymeric matrix may influence the temporal cellular response of the scaffold system, potentially through differences in local drug distribution and exposure [65]. Nevertheless, definitive mechanistic interpretation requires correlation with independent drug-release studies and complementary biological analyses [66].

Research Perspectives

The observed relationships among nanofibrous microstructure, chemical characteristics, thermal behavior, and time-dependent biological response highlight several promising directions for future investigations.

Since incorporation of sodium alginate and Aloe vera into electrospinning formulations can be limited by reduced processability and rheological instability, future studies may focus on optimizing solution properties through auxiliary polymer systems, conductivity modulation, or advanced electrospinning approaches. Such strategies may enable higher incorporation of

bioactive components while preserving fiber continuity, structural homogeneity, and electrospinning stability, thereby improving control over the structural and compositional characteristics of the resulting scaffold systems.

The integration of 3D-printed macroporous substrates with electrospun nanofibrous layers generated a hierarchical multiscale architecture. Future development of synchronized or integrated fabrication platforms combining additive manufacturing and electrospinning may improve interfacial adhesion between layers, reduce structural heterogeneity, and enhance fabrication reproducibility. In addition, such systems may provide more precise control over pore geometry, fiber deposition, and overall scaffold architecture.

Although the present study primarily focused on structural, chemical, thermal, and biological characterization, further mechanical evaluation of hybrid scaffolds is necessary. Investigation of tensile, compressive, and interfacial mechanical behavior would provide valuable insight into the relationship between nanofiber density, layer uniformity, scaffold architecture, and structural stability under relevant physiological-like conditions.

From a biological perspective, the tetrazolium salt–based assay demonstrated time-dependent variations in cellular metabolic activity associated with scaffold composition and drug-loading strategy. However, complementary biological analyses—including cell adhesion studies, fluorescence imaging, live/dead assays, cytoskeletal organization, and long-term proliferation assessments—would provide a more comprehensive understanding of cell–scaffold interactions and the potential influence of multiscale architecture on cellular behavior.

Furthermore, correlation of biological findings with independent drug-release studies would clarify the role of ciprofloxacin localization in affecting temporal cellular responses and local exposure dynamics within the polymeric matrix.

Finally, considering the observed differences in fiber diameter, network density, and structural uniformity among scaffold groups, future studies may investigate nanofiber thickness, deposition density, and multilayer organization as independent design parameters. Such optimization could provide additional control over structural integrity, degradation behavior, drug-release characteristics, and biological performance for advanced tissue engineering and drug-delivery applications.

Acknowledgements

The authors would like to express their sincere gratitude to Dr. Adeleh Gholipour-Kanani for her valuable guidance and support throughout this study.

The authors also acknowledge the Science and Research Branch, Islamic Azad University, Tehran, Iran, for providing academic and research support.

In addition, the authors gratefully acknowledge the Iran Polymer and Petrochemical Institute (IPPI), Tehran, Iran, for providing technical facilities, equipment, and support for the design and fabrication of the three-dimensional printed scaffolds used in this research.

Reference

1. Roddy E, DeBaun M, Daoud A, Yang Y, Gardner M. Treatment of critical-sized bone defects: clinical and tissue engineering perspectives. European Journal of Orthopaedic Surgery & Traumatology. 2018;28. doi: 10.1007/s00590-017-2063-0.
2. Koushik TM, Miller CM, Antunes E. Bone Tissue Engineering Scaffolds: Function of Multi-Material Hierarchically Structured Scaffolds. Adv Healthc Mater. 2023;12(9):e2202766. doi: 10.1002/adhm.202202766.
3. Hossen SMM, Khaleque MA, Lim MS, Kang JK, Kim DK, Lee HH, et al. Biomimetic Strategies for Bone Regeneration: Smart Scaffolds and Multiscale Cues. Biomimetics (Basel). 2025;11(1). doi: 10.3390/biomimetics11010012.
4. Bhushan S, Singh S, Maiti TK, Sharma C, Dutt D, Sharma S, et al. Scaffold Fabrication Techniques of Biomaterials for Bone Tissue Engineering: A Critical Review. Bioengineering (Basel). 2022;9(12). doi: 10.3390/bioengineering9120728.

5. Jang J-W, Min K-E, Kim C, Shin J, Lee J, Yi S. Review: Scaffold Characteristics, Fabrication Methods, and Biomaterials for the Bone Tissue Engineering. International Journal of Precision Engineering and Manufacturing. 2023;24(3):511-29. doi: 10.1007/s12541-022-00755-7.
6. Huang D, Li Z, Li G, Zhou F, Wang G, Ren X, et al. Biomimetic structural design in 3D-printed scaffolds for bone tissue engineering. Materials Today Bio. 2025;32:101664. doi: https://doi.org/10.1016/j.mtbio.2025.101664.
7. Sadjadi S, Rezadoust AM, Yaghoubi S, Monflier E, Heydari A. 3D-Printed Cyclodextrin Polymer Encapsulated Wells–Dawson: A Novel Catalyst for Knoevenagel Condensation Reactions. ACS Omega. 2023;8(48):45844-53. doi: 10.1021/acsomega.3c06592.
8. Gharibshahian M, Salehi M, Beheshtizadeh N, Kamalabadi-Farahani M, Atashi A, Nourbakhsh M-S, et al. Recent advances on 3D-printed PCL-based composite scaffolds for bone tissue engineering. Frontiers in Bioengineering and Biotechnology. 2023;Volume 11 - 2023. doi: 10.3389/fbioe.2023.1168504.
9. Menarbazari AA, Mansoori-Kermani A, Mashayekhan S, Soleimani A. 3D-printed polycaprolactone/tricalcium silicate scaffolds modified with decellularized bone ECM-oxidized alginate for bone tissue engineering. Int J Biol Macromol. 2024;265(Pt 1):130827. doi: 10.1016/j.ijbiomac.2024.130827.
10. Huang T, Zeng Y, Li C, Zhou Z, Xu J, Wang L, et al. Application and Development of Electrospun Nanofiber Scaffolds for Bone Tissue Engineering. ACS Biomater Sci Eng. 2024;10(7):4114-44. doi: 10.1021/acsbiomaterials.4c00028.
11. Zhou X, Wang Y, Ji C. Advances in Preparation and Biomedical Applications of Sodium Alginate-Based Electrospun Nanofibers. Gels. 2025 doi: 10.3390/gels11090704.
12. Islam MS, Karim MR. Fabrication and characterization of poly(vinyl alcohol)/alginate blend nanofibers by electrospinning method. Colloids and Surfaces A: Physicochemical and Engineering Aspects. 2010;366(1):135-40. doi: https://doi.org/10.1016/j.colsurfa.2010.05.038.
13. Dehghan F, Gholipour-Kanani A, Kamali Dolatabadi M, Bahrami SH. Nanofibrous composite from polycaprolactone-polyethylene glycol-aloe vera as a promising scaffold for bone repairing. Journal of Applied Polymer Science. 2022;139(26):e52463. doi: https://doi.org/10.1002/app.52463.
14. Huang B, Aslan E, Jiang Z, Daskalakis E, Jiao M, Aldalbahi A, et al. Engineered dual-scale poly (ε-caprolactone) scaffolds using 3D printing and rotational electrospinning for bone tissue regeneration. Additive Manufacturing. 2020;36:101452. doi: https://doi.org/10.1016/j.addma.2020.101452.

15. Carranza T, Uranga J, Irastorza A, Izeta A, Guerrero P, de la Caba K. Combination of 3D printing and electrospinning to develop chitin/gelatin/PVA scaffolds. Int J Bioprint. 2023;9(3):701. doi: 10.18063/ijb.701.
16. Stone SA, Gosavi P, Athauda TJ, Ozer RR. In situ citric acid crosslinking of alginate/polyvinyl alcohol electrospun nanofibers. Materials Letters. 2013;112:32-5. doi: https://doi.org/10.1016/j.matlet.2013.08.100.
17. Neto JdFG, Pinto Moura B, Lima TdPdL, Marega FM, Pinto LA, Granja PL, et al. Synergistic Effects of Ceramic Fillers and NaOH Treatment on Bioactivity of 3D-Printed Poly(ε-caprolactone) Scaffolds for Periodontal Tissue Regeneration. ACS Omega. 2026;11(4):5508-25. doi: 10.1021/acsomega.5c09061.
18. Pasieczna-Patkowska S, Cichy M, Flieger J. Application of Fourier Transform Infrared (FTIR) Spectroscopy in Characterization of Green Synthesized Nanoparticles. Molecules. 2025;30(3). doi: 10.3390/molecules30030684.
19. Iga C, Agata T, Marcin Ł, Natalia F, Justyna KL. Ciprofloxacin-Modified Degradable Hybrid Polyurethane-Polylactide Porous Scaffolds Developed for Potential Use as an Antibacterial Scaffold for Regeneration of Skin. Polymers (Basel). 2020;12(1). doi: 10.3390/polym12010171.
20. Mosmann T. Rapid colorimetric assay for cellular growth and survival: Application to proliferation and cytotoxicity assays. Journal of Immunological Methods. 1983;65(1):55-63. doi: https://doi.org/10.1016/0022-1759(83)90303-4.
21. Rošic R, Pelipenko J, Kristl J, Kocbek P, Bešter-Rogač M, Baumgartner S. Physical characteristics of poly (vinyl alcohol) solutions in relation to electrospun nanofiber formation. European Polymer Journal. 2013;49(2):290-8. doi: https://doi.org/10.1016/j.eurpolymj.2012.11.013.
22. Nie H, He A, Zheng J, Xu S, Li J, Han CC. Effects of chain conformation and entanglement on the electrospinning of pure alginate. Biomacromolecules. 2008;9(5):1362-5. doi: 10.1021/bm701349j.
23. Jadbabaei S, Kolahdoozan M, Naeimi F, Ebadi-Dehaghani H. Preparation and characterization of sodium alginate-PVA polymeric scaffolds by electrospinning method for skin tissue engineering applications. RSC Adv. 2021;11(49):30674-88. doi: 10.1039/d1ra04176b.
24. Xia P, Luo Y. Vascularization in tissue engineering: The architecture cues of pores in scaffolds. J Biomed Mater Res B Appl Biomater. 2022;110(5):1206-14. doi: 10.1002/jbm.b.34979.
25. Isfahani FR, Tavanai H, Morshed M. Release of aloe vera from electrospun aloe vera-PVA nanofibrous pad. Fibers and Polymers. 2017;18(2):264-71. doi: 10.1007/s12221-017-6954-9.

26. Uhljar L, Kan SY, Radacsi N, Koutsos V, Szabó-Révész P, Ambrus R. In Vitro Drug Release, Permeability, and Structural Test of Ciprofloxacin-Loaded Nanofibers. Pharmaceutics. 2021;13(4). doi: 10.3390/pharmaceutics13040556.
27. Nayak R, Padhye R, Kyratzis IL, Truong YB, Arnold L. Effect of viscosity and electrical conductivity on the morphology and fiber diameter in melt electrospinning of polypropylene. Textile Research Journal. 2013;83(6):606-17. doi: 10.1177/0040517512458347.
28. Syed Abdullah SS, Faisul Aris FA, Said Azmi SNN, Anak John JHS, Khairul Anuar NN, Mohd Asnawi ASF. Development and evaluation of ciprofloxacin-bacterial cellulose composites produced through in situ incorporation method. Biotechnol Rep (Amst). 2022;34:e00726. doi: 10.1016/j.btre.2022.e00726.
29. Gaydhane MK, Sharma CS, Majumdar S. Electrospun nanofibres in drug delivery: advances in controlled release strategies. RSC Adv. 2023;13(11):7312-28. doi: 10.1039/d2ra06023j.
30. McKee MG, Hunley MT, Layman JM, Long TE. Solution Rheological Behavior and Electrospinning of Cationic Polyelectrolytes. Macromolecules. 2006;39(2):575-83. doi: 10.1021/ma051786u.
31. Sohail N, Fischer T, Martienssen M. Enhanced Durability of Cellulose-Reinforced PVA-SA Beads for Long-Term Quorum Quenching Applications in Membrane Bioreactors. Gels. 2026;12(6):480.
32. Phillipson K, Hay JN, Jenkins MJ. Thermal analysis FTIR spectroscopy of poly(ε-caprolactone). Thermochimica Acta. 2014;595:74-82. doi: https://doi.org/10.1016/j.tca.2014.08.027.
33. Wilpiszewska K, Antosik AK, Zdanowicz M. The Effect of Citric Acid on Physicochemical Properties of Hydrophilic Carboxymethyl Starch-Based Films. Journal of Polymers and the Environment. 2019;27(6):1379-87. doi: 10.1007/s10924-019-01436-9.
34. Hsiao KY, Chung RJ, Chang PP, Tsai TH. Identification of Hydroxyl and Polysiloxane Compounds via Infrared Absorption Spectroscopy with Targeted Noise Analysis. Polymers (Basel). 2025;17(11). doi: 10.3390/polym17111533.
35. Chelu M, Popa M, Ozon EA, Pandele Cusu J, Anastasescu M, Surdu VA, et al. High-Content Aloe vera Based Hydrogels: Physicochemical and Pharmaceutical Properties. Polymers (Basel). 2023;15(5). doi: 10.3390/polym15051312.
36. Bialik-Wąs K, Raftopoulos KN, Pielichowski K. Alginate Hydrogels with Aloe vera: The Effects of Reaction Temperature on Morphology and Thermal Properties. Materials. 2022;15(3):748.

37. Bajer D, Janczak K, Bajer K. Novel Starch/Chitosan/Aloe Vera Composites as Promising Biopackaging Materials. Journal of Polymers and the Environment. 2020;28(3):1021-39. doi: 10.1007/s10924-020-01661-7.
38. García MC, Cuggino JC, Rosset CI, Páez PL, Strumia MC, Manzo RH, et al. A novel gel based on an ionic complex from a dendronized polymer and ciprofloxacin: Evaluation of its use for controlled topical drug release. Mater Sci Eng C Mater Biol Appl. 2016;69:236-46. doi: 10.1016/j.msec.2016.06.071.
39. Sirivisoot S, Harrison BS. Magnetically stimulated ciprofloxacin release from polymeric microspheres entrapping iron oxide nanoparticles. International Journal of Nanomedicine. 2015;10(null):4447-58. doi: 10.2147/IJN.S82830.
40. Ibrahim MA, Nasr GM, Ahmed RM, Kelany NA. Physical characterization, biocompatibility, and antimicrobial activity of polyvinyl alcohol/sodium alginate blend doped with TiO2 nanoparticles for wound dressing applications. Scientific Reports. 2024;14(1):5391. doi: 10.1038/s41598-024-55818-8.
41. Ueno T, Nakashima E, Takeda K. Quantitative analysis of random scission and chain-end scission in the thermal degradation of polyethylene. Polymer Degradation and Stability. 2010;95(9):1862-9. doi: https://doi.org/10.1016/j.polymdegradstab.2010.04.020.
42. Chelu M, Popa M, Ozon EA, Pandele Cusu J, Anastasescu M, Surdu VA, et al. High-Content Aloe vera Based Hydrogels: Physicochemical and Pharmaceutical Properties. Polymers. 2023;15(5):1312.
43. Alvarenga BRd, Jr., Moseson DE, Carneiro RL, Taylor LS. Impact of Polymer Type on Thermal Degradation of Amorphous Solid Dispersions Containing Ritonavir. Molecular Pharmaceutics. 2022;19(1):332-44. doi: 10.1021/acs.molpharmaceut.1c00823.
44. J. McCoy B. Polymer thermogravimetric analysis: effects of chain-end and reversible random scission. Chemical Engineering Science. 2001;56(4):1525-9. doi: https://doi.org/10.1016/S0009-2509(00)00379-1.
45. Arunachalam K, Sreeja PS. MTT Assay Protocol. In: Arunachalam K, Sreeja PS, editors. Advanced Cell and Molecular Techniques: Protocols for In Vitro and In Vivo Studies. New York, NY: Springer US; 2025. p. 271-6.
46. Ghasemi M, Turnbull T, Sebastian S, Kempson I. The MTT Assay: Utility, Limitations, Pitfalls, and Interpretation in Bulk and Single-Cell Analysis. Int J Mol Sci. 2021;22(23). doi: 10.3390/ijms222312827.
47. Klimek K, Terpilowska S, Michalak A, Bernacki R, Nurzynska A, Cucchiarini M, et al. Modern Approach to Testing the Biocompatibility of Osteochondral Scaffolds in Accordance with the 3Rs Principle–Preclinical In Vitro, Ex Vivo, and In Vivo

Studies Using the Biphasic Curdlan-Based Biomaterial. ACS Biomater Sci Eng. 2025;11(2):845-65. doi: 10.1021/acsbiomaterials.4c01107.
48. Rancan F, Contardi M, Jurisch J, Blume-Peytavi U, Vogt A, Bayer IS, et al. Evaluation of Drug Delivery and Efficacy of Ciprofloxacin-Loaded Povidone Foils and Nanofiber Mats in a Wound-Infection Model Based on Ex Vivo Human Skin. Pharmaceutics. 2019;11(10):527.
49. Krishnan AG, Jayaram L, Biswas R, Nair M. Evaluation of Antibacterial Activity and Cytocompatibility of Ciprofloxacin Loaded Gelatin–Hydroxyapatite Scaffolds as a Local Drug Delivery System for Osteomyelitis Treatment. Tissue Engineering Part A. 2015;21(7-8):1422-31. doi: 10.1089/ten.tea.2014.0605.
50. Wang S, Yu H, Wickliffe JK. Limitation of the MTT and XTT assays for measuring cell viability due to superoxide formation induced by nano-scale TiO2. Toxicol In Vitro. 2011;25(8):2147-51. doi: 10.1016/j.tiv.2011.07.007.
51. Zhang X, Wang T, Zhang Z, Liu H, Li L, Wang A, et al. Electrical stimulation system based on electroactive biomaterials for bone tissue engineering. Materials Today. 2023;68:177-203. doi: https://doi.org/10.1016/j.mattod.2023.06.011.
52. Carrasco-Rojas J, Sandoval FI, Solas-Soto J, Schuh CMAP, Rubio-Quiroz L, Lagos CF, et al. Nanostructured Lipid Carriers Enhance Ciprofloxacin Antibacterial Activity Through Diffusion-Controlled Release and Modulation of Bacterial Growth Kinetics. Pharmaceutics. 2026;18(4):496.
53. Xiang Z, Sarazin P, Favis BD. Controlling Burst and Final Drug Release Times from Porous Polylactide Devices Derived from Co-continuous Polymer Blends. Biomacromolecules. 2009;10(8):2053-66. doi: 10.1021/bm8013632.
54. Ceballos-Santa MC, Sierra A, Zalbidea IM, Lazarus E, Marin-Montealegre V, Ramesh S, et al. Aloe vera-based biomaterial ink for 3D bioprinting of wound dressing constructs. J Biomed Mater Res B Appl Biomater. 2024;112(2):e35379. doi: 10.1002/jbm.b.35379.
55. Vigata M, Meinert C, Hutmacher DW, Bock N. Hydrogels as Drug Delivery Systems: A Review of Current Characterization and Evaluation Techniques. Pharmaceutics. 2020;12(12):1188.
56. Safi S, Morshed M, Hosseini Ravandi SA, Ghiaci M. Study of electrospinning of sodium alginate, blended solutions of sodium alginate/poly(vinyl alcohol) and sodium alginate/poly(ethylene oxide). Journal of Applied Polymer Science. 2007;104(5):3245-55. doi: https://doi.org/10.1002/app.25696.
57. Taemeh MA, Shiravandi A, Korayem MA, Daemi H. Fabrication challenges and trends in biomedical applications of alginate electrospun nanofibers. Carbohydr Polym. 2020;228:115419. doi: 10.1016/j.carbpol.2019.115419.

58. McKee MG, Wilkes GL, Colby RH, Long TE. Correlations of Solution Rheology with Electrospun Fiber Formation of Linear and Branched Polyesters. Macromolecules. 2004;37(5):1760-7. doi: 10.1021/ma035689h.
59. El-hadi AM, Al-Jabri FY. Influence of Electrospinning Parameters on Fiber Diameter and Mechanical Properties of Poly(3-Hydroxybutyrate) (PHB) and Polyanilines (PANI) Blends. Polymers. 2016;8(3):97.
60. Jiang N, Qi B, Fan X, Yao L, Wang Y, Zhao Z, et al. Fabrication of biocompatible and biodegradable polyvinyl alcohol/sodium alginate blend polymers incorporating Ca2+ doped TiO2 nanocomposite 3D scaffold for biomedical applications. Journal of Saudi Chemical Society. 2023;27(6):101758. doi: https://doi.org/10.1016/j.jscs.2023.101758.
61. Yumin A, Liguo D, Yi Y, Yongna J. Mechanical properties of an interpenetrating network poly(vinyl alcohol)/alginate hydrogel with hierarchical fibrous structures. RSC Advances. 2022;12(19):11632-9. doi: 10.1039/d1ra07368k.
62. Shah A, Saqib M, Asim M, Ismail B, Alamri MA, Rehman W. Structural and interfacial characterization of ciprofloxacin-loaded starch/HPMC sepiolite nanocomposite films. RSC Advances. 2026;16(24):22092-104. doi: 10.1039/d6ra02229d.
63. Maniruzzaman M, Morgan DJ, Mendham AP, Pang J, Snowden MJ, Douroumis D. Drug–polymer intermolecular interactions in hot-melt extruded solid dispersions. International Journal of Pharmaceutics. 2013;443(1):199-208. doi: https://doi.org/10.1016/j.ijpharm.2012.11.048.
64. Mamin EA, Pantyukhov PV, Olkhov AA. Oxo-Additives for Polyolefin Degradation: Kinetics and Mechanism. Macromol. 2023;3(3):477-506.
65. Krishnan AG, Jayaram L, Biswas R, Nair M. Evaluation of antibacterial activity and cytocompatibility of ciprofloxacin loaded gelatin-hydroxyapatite scaffolds as a local drug delivery system for osteomyelitis treatment. Tissue Eng Part A. 2015;21(7-8):1422-31. doi: 10.1089/ten.TEA.2014.0605.
66. Onaciu A, Munteanu RA, Moldovan AI, Moldovan CS, Berindan-Neagoe I. Hydrogels Based Drug Delivery Synthesis, Characterization and Administration. Pharmaceutics. 2019;11(9):432.